



Local stability of WF sections in fire

Gabrielle Pomerleau¹, Jeanne Paquet², Nicolas Boissonnade³

Abstract

The local buckling behavior of hot-rolled and welded I-sections under simple load cases at elevated temperatures is investigated numerically through extensive numerical analysis. Advanced shell Finite Element (F.E.) models are firstly developed and validated against existing experimental data for I-sections under fire conditions. These validated models are subsequently used to conduct extensive parametric studies encompassing a wide range of cross-section geometries, steel grades and temperatures. The reference F.E. results are then compared with resistances predicted by the current European provisions. It is shown that these design provisions, which rely on similar cross-section classification and on the Effective Width Method (E.W.M.) just as room temperature rules, provide over-conservative and scattered resistance predictions to various extents. Therefore, an alternative design method – the Overall Interaction Concept (O.I.C.) – is proposed in this paper for I-sections at elevated temperatures. The O.I.C. is evidenced to provide more accurate, consistent and straightforward resistance predictions than current standards. Eventually, the reliability levels associated with the O.I.C.-based design methodology and the current European provisions are evaluated.

1. Introduction

Steel members with I-section geometries are widely employed in building applications and in bridge construction since I-sections can be easily manufactured and connected with other components. I-sections are highly efficient in resisting bending and shear loads; however, their performance under minor-axis bending is relatively limited, and they exhibit low torsional stiffness, which might accelerate the occurrence of lateral buckling. Besides, for thin-walled I-sections, the occurrence of local buckling may reduce the stiffness and resistance and further induce global instability which thereby reduces the ultimate resistance of members. In recent years, extensive research has been conducted to investigate the various buckling behaviors of I-sections at ambient temperature, including local buckling [e.g., (Yun et al., 2018b), (Yun et al., 2018c), (Su et al., 2021), (Gérard et al., 2021), (Li et al., 2022), (Chen et al., 2022)], global buckling [(Taras & Greiner, 2008), (Ban & Shi, 2018), (Yan et al., 2020), (Bradford & Liu, 2016)] and local-global coupled instabilities [(Couto & Real, 2019), (Shi et al., 2020), (Li & Boissonnade, 2022)].

¹ MSc student, Laval University, <gabrielle.pomerleau.4@ulaval.ca>

² MSc student, Laval University, <jeanne.paquet.2@ulaval.ca>

³ Professor, Laval University, <nicolas.boissonnade@gci.ulaval.ca>

At elevated temperatures, the buckling behavior of steel I-sections is very different from their response at ambient temperature. When exposed to fire, the elastic modulus and yield strength of steel degrade at different rates with increasing temperature, causing steel sections or members to become more susceptible to buckling. Besides, at high temperatures, the stress-strain relationship of carbon steel becomes distinctly non-linear at relatively low stress levels [(Knobloch et al., 2013), (Knobloch, 2008)]. Additionally, the influence of creep, which becomes noticeable at temperatures exceeding 400 °C, significantly impacts the resistance of steel structures (Kodur & Dwaikat, 2010). Consequently, design formulae dedicated to steel sections or members at room temperature cannot be straightforwardly adapted to fire design by merely adjusting material properties such as yield strength and elastic modulus, and further experimental and numerical investigations are needed to correctly characterize the buckling behavior and carrying capacity of I-section members in case of fire.

Over the years, several experimental programs have been carried out with tests being either transient-state or steady-state. In the former case, the specimens are initially loaded at ambient temperature and then temperature is increased until the specimens lose their carrying capacity. As examples, Franssen et al. [(Franssen et al., 2014), (Franssen et al., 2016)] conducted several transient-state tests to investigate the failure modes of slender I-section long columns at elevated temperatures. As for steady-state tests, specimens are heated at a specific temperature before applying loads, which keep increasing up to peak – and even beyond thanks to displacement-controlled techniques. To examine the local instability of mild Q235 steel and high strength Q460 steel welded I-sections, Wang et al. (Wang et al., 2014) tested 12 columns under steady-state conditions at 450 °C and 650 °C. The test results inferred that steel columns with higher yield strength lost their carrying capacities more rapidly. Similar steady-state tests were carried out by other authors, focusing on both hot-rolled sections (Pauli, 2013) and welded sections [(Yang et al., 2006), (Hirashima et Uesugi, 2005), (Hricak et al., 2014), (Prachar et al., 2016)]. These studies examined a variety of structural elements, including columns [(Pauli, 2013), (Yang et al., 2006)], beams [(Hricak et al., 2014), (Prachar et al., 2016)] and beam-columns [(Pauli, 2013), (Hirashima et Uesugi, 2005)]. All these tests indicate that at elevated temperatures, I-section elements are more prone to suffer from local buckling effects than at room temperature; early local buckling prevents sections from reaching their plastic capacity and therefore has a detrimental impact on their load bearing capacity. Further examples of discussions about the experimental tests on steel members under fire are summarized in (Maraveas, 2019).

In addition to experimental studies, many numerical analyses have been performed, providing numerous and accurate estimates of section or member resistances under fire. Among recent contributions, Couto et al. (Couto et al., 2014) developed F.E. models of steel plates at elevated temperatures considering various plate slenderness, steel grades, boundary conditions and loading situations. Their findings revealed that the design rules suggested in existing Eurocode 3 (EC 3) (European Committee for Standardisation, 2007) overestimate the resistance of plate elements for Class 3 sections. Subsequently, these authors proposed new expressions for local buckling at elevated temperatures (Couto et al., 2015) which were incorporated in the revised version of prEN 1993-1-2 (European Committee for Standardisation, 2020) but only for Class 4 sections for which the capacity had previously been underestimated. A few years later, Kucukler (Kucukler, 2021) performed similar analyses and identified that although the latest version of prEN 1993-1-2 (European Committee for Standardisation, 2020) provides safe predictions for normal strength steel plates, the resistances of high strength steel plates, i.e., made in S460 or S690 steel, are still underestimated. This discrepancy arises partly because earlier studies by Couto et al. [(Couto et

al., 2014), (Couto et al., 2016)] only considered steel grades up to S460. Fang and Chan (Fang & Chan, 2018) conducted numerical analyses on the behavior and resistance of welded S460 steel stub and long columns under axial compression. They pointed out that the design rules in current Eurocode 3 (European Committee for Standardisation, 2007) or the American Standards (A.I.S.C.) (AISC, 2010) underestimate the resistance of box and I-section members in fire situations. Instead, Couto et al. [(Couto et al., 2015), (Couto et al., 2016)] and Yun et al. (Yun et al., 2020) concluded that the design rules suggested by these two provisions [(European Committee for Standardisation, 2007), (AISC, 2010)] obviously overestimate carrying capacities for semi-compact cross-sections.

Current code prescriptions for dealing with local buckling of steel sections in fire [(European Committee for Standardisation, 2007), (European Committee for Standardisation, 2020), (AISC, 2010)] usually relies on the cross-section classification system and on the Effective Width Method (E.W.M.); typically, only minimum modifications on design equations for ambient temperature are provided to account for reduced mechanical properties of steel at elevated temperatures. The design procedures provided by Eurocode 3 [(European Committee for Standardisation, 2007), (European Committee for Standardisation, 2020)] and the American Standards (AISC, 2010) for predicting cross-section resistance in case of fire have been summarized and compared with existing experimental or numerical results in [(Kucukler, 2021), (Fang & Chan, 2018), (Yun et al., 2020), (Couto et al. 2021)]. It was evidenced that these design methods do not properly capture the non-linear stress-strain relationship of steel at high temperatures and therefore may result in inaccurate and inconsistent resistance predictions [(Couto et al., 2015), (Couto et al., 2016), (Fang & Chan, 2018), (Yun et al., 2020), (Couto et al. 2021)]. Accordingly, more accurate and improved approaches for steel sections in fire have been developed in recent years. A strain-based approach, the Continuous Strength Method (C.S.M.), which was originally designed to take advantage of strain hardening benefits in stainless steel compact sections (Afshan & Gardner, 2013), was recently extended to the fire design of steel hollow sections under simple load cases (Theofanous et al., 2016) or combined load cases (Yun et al., 2020). Besides, the Direct Strength Method (D.S.M.), which was developed for the design of cold-formed steel members at ambient temperature (Schafer, 2008), was found to provide inaccurate resistance predictions for stub columns at elevated temperatures [(Fang & Chan, 2018), (Couto et al. 2021)], and modified D.S.M. procedures were provided in [(Fang & Chan, 2018), (Chen & Young, 2008)] for high strength steel box and I-section columns.

Similar to the C.S.M. and the D.S.M., the Overall Interaction Concept (O.I.C.) (Boissonnade et al., 2017) does not rely on the classification concept nor on the E.W.M., yet unlike the D.S.M., the O.I.C. keeps the section plastic capacity as a reference. The O.I.C. further accounts for the effects of imperfections and their interactions with material yielding and buckling through buckling curves, such as the ones suggested in Eurocode 3 (European Committee for Standardisation, 2005) for column buckling. The O.I.C. however generalizes the use of such buckling curves to section resistance, with $\chi_L = f^o(\lambda_L)$ local buckling curves to predict cross-section resistance.

The application steps of O.I.C. are presented in Fig. 1, where three key load ratios, i.e., plastic load ratio R_{pl} , local elastic critical load ratio $R_{cr,L}$ and ultimate resistance load ratio $R_{b,L}$, are evidenced. Each of these load ratios shall be understood as the factor by which the initial loading has to be multiplied to reach its corresponding limit case, i.e. the plastic limit state (all fibers yielded yet no buckling), the local buckling limit case (no yielding) or the ultimate limit state (“real” carrying capacity, including the effects of both yielding, buckling, initial imperfections and their interactions). Note that two such ratios, R_{pl} and $R_{cr,L}$, can be calculated by approximate formulae,

such as suggested in current provisions [(European Committee for Standardisation, 2007), (AISC, 2010), (European Committee for Standardisation, 2006)] or in classical textbooks [(Timoshenko & Gere, 1963), (Petersen, 2012), (Petersen, 2020), (Eng et al., 2011), (Ziemian, 2010)] or by specific tools (Boissonnade et al., 2017). After calculating the cross-section slenderness λ_L (Fig. 1), a local buckling reduction factor χ_L is determined using a local buckling curve for the cross-section. This curve accounts for the effects of material yielding, local buckling, imperfections and their interactions. Finally, the ultimate load ratio $R_{b,L}$ is obtained, and a final resistance design check ensuring safety consists in $R_{b,L} \geq 1.0$, indicating that the actual applied loading shall be increased for failure to occur. More details on the underlying mechanical principles and characteristics of the O.I.C. can be found in (Boissonnade et al., 2017).

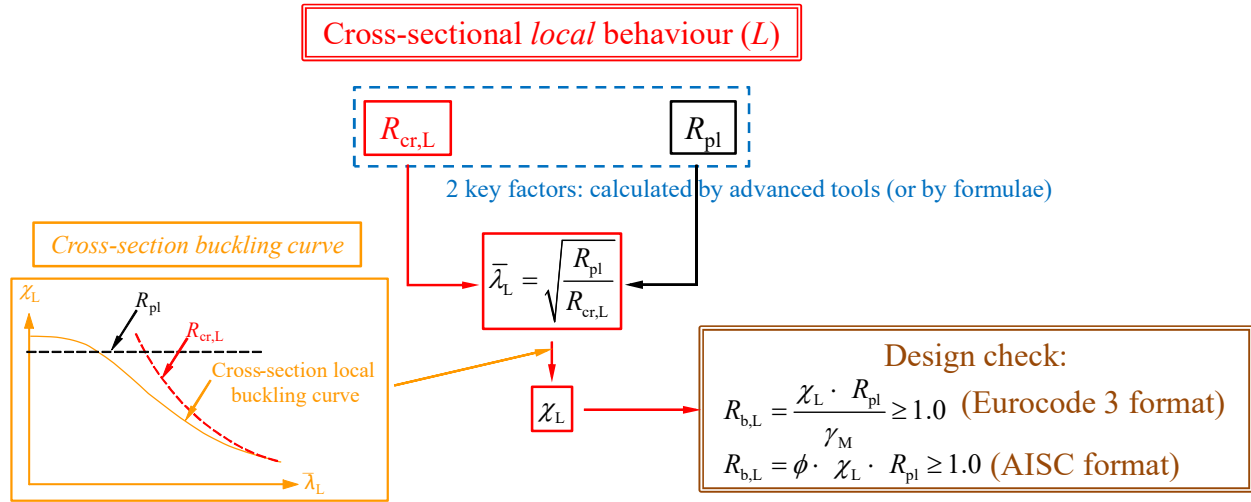


Figure 1: O.I.C. design flow chart for cross section resistance.

The O.I.C. has been first developed for hollow sections and open sections and members at room temperature [(Gérard et al., 2021), (Li & Boissonnade, 2022), (Boissonnade et al., 2017), (Hayeck, 2016), (Nseir, 2015), (Saloumi et al., 2020), (Hayeck et al., 2018)], and this paper aims at extending the O.I.C. to hot-rolled and welded I-sections under simple load cases in the case of fire. Firstly, Section 2 provides a detailed description of the non-linear shell numerical models developed and used in this research. These F.E. models are validated against steady-state experimental results reported by Pauli (Pauli, 2013) and Hricak (Hricak et al., 2014) and are then used to perform extensive parametric studies (Section 3) to consider a wider scope of cross-section geometries, cross-section slenderness, yield limits and fire temperatures. Based on the resulting numerical results, Section 4 introduces a series of O.I.C. cross-section buckling curves for both hot-rolled sections and welded sections. The resistances predicted by O.I.C. proposals and by the European Standards are compared to numerical results in Section 5, allowing a critical evaluation of the proposed approach relative to existing design rules.

2 Numerical modeling

2.1 Basic features of shell F.E. models

Numerical investigations on hot-rolled and welded steel I-sections under simple load cases in fire were processed through general-purpose F.E. software ABAQUS (Abaqus, 2011). Advanced numerical models developed in previous studies [(Li et al., 2022a), (Li et al., 2022b), (Li et al., 2022c)] for characterizing the resistance of I-sections at ambient temperature were adjusted to

carefully account for the properties of carbon steel at elevated temperatures. Therefore, only key modeling features are described herein.

The 4-node quadrilateral shell element with reduced integration S4R, which has been used in many previous studies [(Fang & Chan, 2018), (Yun et al., 2020), (Yin & Wang, 2004)] to study steel cross-sections and members at elevated temperatures, was also selected for the numerical models used in this paper’s investigations. Geometrically and Materially Non-linear with Imperfections Analyzes (G.M.N.I.A.) were performed to calculate ultimate resistances of I-sections by means of the “Riks method”. Following preliminary results relative to mesh density analyses, a relative mesh size equal to $1 / 24^{\text{th}}$ of the web height [(Li et al., 2022b), (Li et al., 2022)] was adopted to discretize each plate element (i.e., web or flange). Besides, for hot-rolled sections, extra hollow beam and spring elements were considered in web-to-flange zones to simulate real geometries in the fillet areas [(Gérard et al., 2021), (Li et al., 2022), (Li et Boissonnade, 2022c), (Gérard et al., 2019)], in order to (i) better account for the actual section geometry and to (ii) provide extra torsional rigidity (see Fig. 2). The dimensions of the hollow beam section are defined by Eqs. (1) and (2), where A_{beam} is the area of the two hollow beam sections, A_{radius} is the area of two radius zones, A_{overlap} is the overlap area at the web-flange intersection. $I_{t,\text{beam}}$, $I_{t,\text{real}}$ and $I_{t,\text{plates}}$ represent the torsional constants of the hollow beam section, of the real I-section and of the section only made of three plates (two flanges and web), respectively – note that the 0.5 factor in Eq. (2) accounts for 2 web-flange intersections (top and bottom).

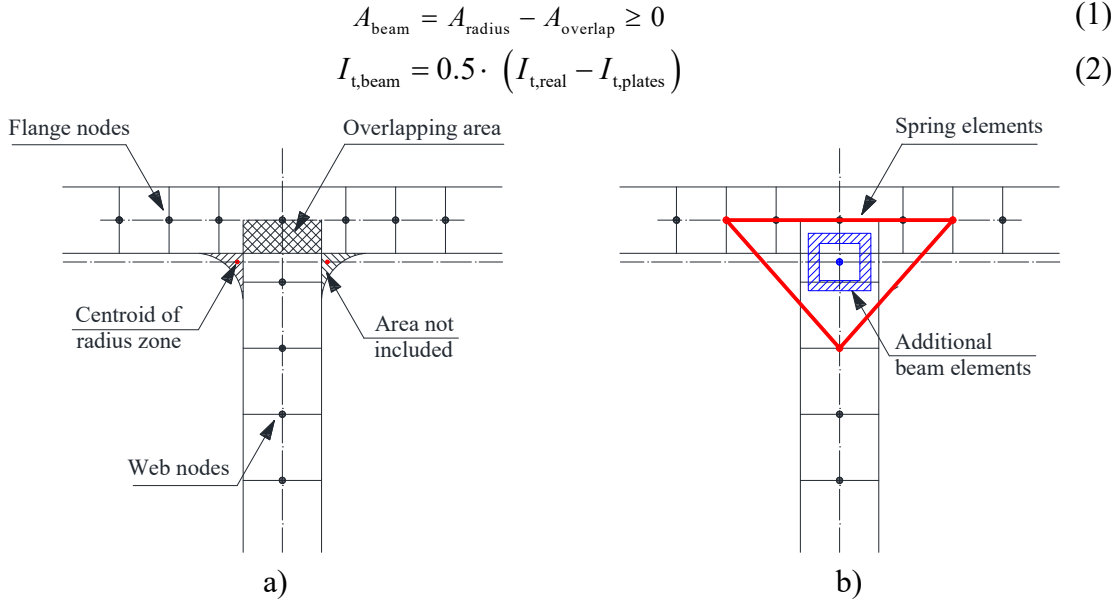


Figure 2: Web-to-flange area of hot-rolled sections – a) Real geometry – b) Modelled geometry.

To replicate numerically the experimental support conditions, the nodes at end-sections were constrained to reference points through rigid body constraints as shown in Fig. 3. Nodal forces, i.e., N or M_y , were applied at reference points to induce compression loads or bending moments. These forces were distributed evenly across the sections due to the kinematic constraints, consistent with Bernoulli’s assumption. Horizontal displacements U_y and U_z and rotation θ_x of both reference points were restrained. In addition, for centrally loaded stub columns (Pauli, 2013) with fixed-end boundary conditions, rotations θ_y and θ_z were prevented as well. For eccentrically-loaded stub columns (Pauli, 2013), rotations about the axis of bending were set free to simulate

pin-ended boundary conditions. Load eccentricities about y and z axes were defined by e_y and e_z , respectively, and the e_x distances between supports and end-sections account for the true position where bending rotations are acting, introducing a certain longitudinal shift.

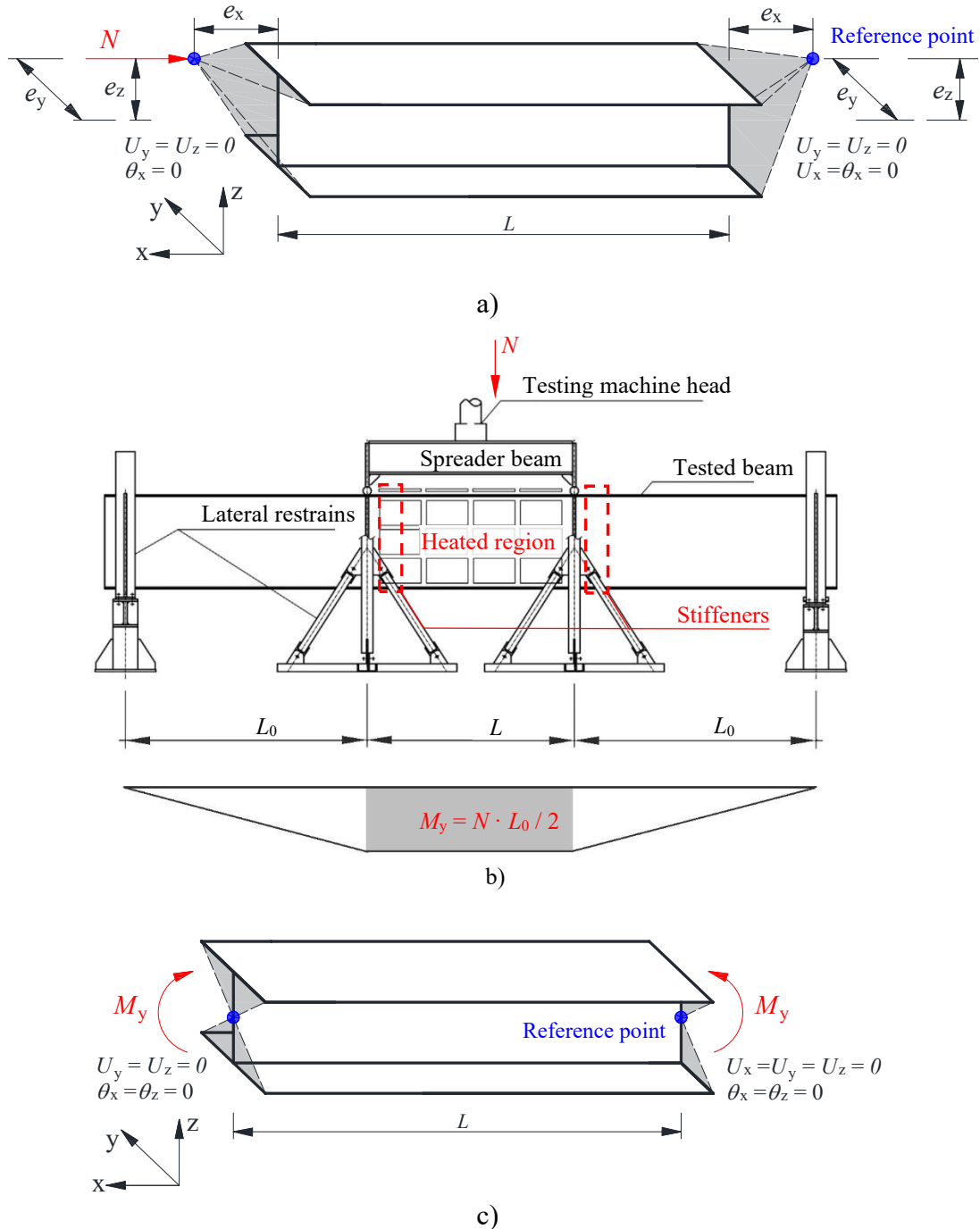


Figure 3: Boundary conditions and load application – a) Stub column model – b) Four-point bending test set-up in (Hricak et al., 2014) – c) Pure bending model.

Furthermore, another “pure bending” F.E. model whose length was equal to the segment of length L under constant bending moment was developed to validate the four-point bending tests (Hricak et al., 2014). Note that for each of the tested beams in (Hricak et al., 2014), web stiffeners were located at the positions where the loads were applied, so that local buckling deformations at the extremities of the loaded panel were prevented. Similar beam models subjected to pure bending moment were generated in (Yun et al., 2018) to validated against four-point bending tests.

The engineering stress-strain curves measured by (Pauli, 2013) were transformed into true stress and logarithmic plastic strain curves for implementation in ABAQUS. As for the tests reported in (Hricak et al., 2014), where only key material properties from tensile coupon tests have been provided, the non-linear material response of carbon steel at elevated temperatures was considered in numerical models by incorporating the key material properties into the stress-strain curve equations suggested by EN 1993-1-2 (European Committee for Standardisation, 2007) as reproduced in Fig. 4a. In this graph, $E_{a,\theta}$ is the Young's modulus of carbon steel at elevated temperatures, $\varepsilon_{p,\theta}$ and $f_{p,\theta}$ are the strain and stress at proportional limits, respectively, and $\varepsilon_{y,\theta}$ and $f_{y,\theta}$ are effective yield strain and stress at elevated temperatures. The values of $E_{a,\theta}$, $f_{p,\theta}$ and $f_{y,\theta}$ are relative to their corresponding values at ambient temperature (see Fig. 4b). Further details regarding Fig. 4 will be provided in Sections 3 and 5. Note that ongoing research is focused on enhancing constitutive models for high-strength steels at elevated temperatures to better characterize their behavior under fire conditions [(Chen et al., 2006), (Xiong & Liew, 2016), (Choi et al., 2014)]. The influence of these improved material models on the proposed equations will be explored and discussed in future studies.

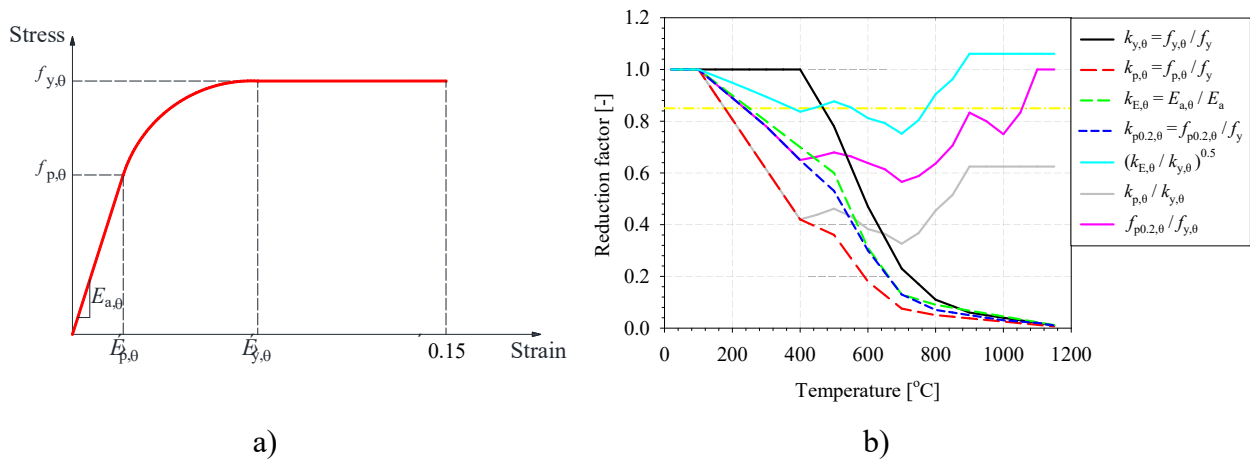


Figure 4: Material law adopted in numerical models – a) Stress-strain relationship – b) Reduction factors.

Local geometrical imperfections were incorporated in the F.E. models by modifying nodes coordinates through sinusoidal functions [(Gérard et al., 2021), (Li et Boissonnade, 2022), (Hayeck et al., 2018), (Gérard et al., 2019), (Gérard, 2020), (Johansson et al., 2007)] as shown in Fig. 5, where $a_{local,f}$ and $a_{local,w}$ represent the amplitudes in web and flange plates, respectively. Prior to the F.E. parametric studies detailed in Section 3, the influence of imperfections’ amplitudes on section resistance was analyzed. Four sets of $a_{local,f}$ and $a_{local,w}$ values have been considered in numerical models: the measured local imperfection amplitudes $a_{measured}$ recorded in [(Pauli, 2013), (Hricak et al., 2014)] and three fractions of each individual “plate buckling length a_i ”, i.e., $a_i / 400$,

$a_i / 200$ and $a_i / 100$, where the a_i 's are defined as flat lengths in web and flanges, so that $a_i = h - 2 t_f - 2 r$ for web plates and $a_i = b - t_w - 2 r$ for flange plates.

The length of the I-shaped members in the numerical models was defined to be sufficiently long to eliminate the influence of end supports while being short enough to ensure that member (global) buckling was negligible, i.e., only local buckling is relevant. Also, lengths were chosen to be multiples of the half-wavelength (see Fig. 5), and preference was given to an odd number of half-waves to guarantee that the middle section remains the weakest one. Eventually, setting the length of short members to three buckling half-waves showed to be the best compromise [(Gérard et al., 2021), (Li et al., 2022), (Gérard et al., 2019)].

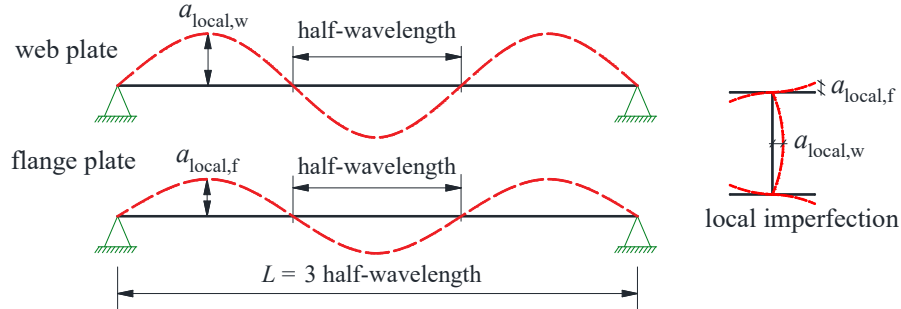


Figure 5: Definition of geometrical (local) imperfections.

Whereas many investigations [(Gérard, 2020), (Galambos & Ketter, 1959), (Ban et al., 2013)] have been conducted to characterize the residual stresses patterns of hot-rolled and welded I-sections at room temperature over the last decade, only limited information is available on residual stresses in the fire situation. Vila Real et al. (Real et al. 2004) numerically analyzed the influence of residual stresses on the lateral-torsional resistance of steel I-beams at elevated temperatures and found that member resistance becomes less sensitive to residual stresses with an increase in fire temperature. More recently, Wang et al. [(Wang et al. 2015), (Wang & Qin, 2016)] and Sun et al. (Sun et al., 2020) measured residual stresses in welded I-sections after fire exposure. Their studies indicated that although the magnitude of residual stresses decreased rapidly, they do not completely disappear and still have detrimental effects on the resistance of sections and members. In addition, according to the studies in (Couto & Real, 2021), although the impact of residual stresses on short members is relatively minor, it is still recommended to model residual stresses consistently in all cases to ensure that all necessary factors are accounted for in the modeling process.

Therefore, in this paper, residual stresses were considered in the F.E. models for both hot-rolled and welded sections by reducing the magnitude of residual stresses patterns for room temperatures [(Gérard et al., 2021), (Li et al., 2022), (Gérard et al., 2019)]. As shown in Fig. 6 and Table 1, the magnitudes relative to the yield strength $f_{y,235}$ or f_y were reduced to stresses at the proportional limit $f_{p,\theta}$ (Type 1) or at the effective yield strength $f_{y,\theta}$ (Type 2). Note that at room temperature, there is limited information available about the distribution of residual stresses in high strength hot-rolled I-sections. While some experiments [(Beg & Kozlevcar, 2007), (Launert et al., 2016)] have suggested that residual stresses patterns in high strength steel welded I-sections may be more favorable, other measurements (Sun et al., 2021) indicated that S690 welded I-sections exhibit a maximum value depending on the yield stress f_y . Accordingly, until clearer guidelines are established for high strength steel, this study adopts the patterns in Fig. 6 and the influence of residual stresses on high strength steel I-sections shall be addressed in future research.

More discussions about the influence of local imperfections and residual stresses on section resistance are provided in the next Section 2.2.

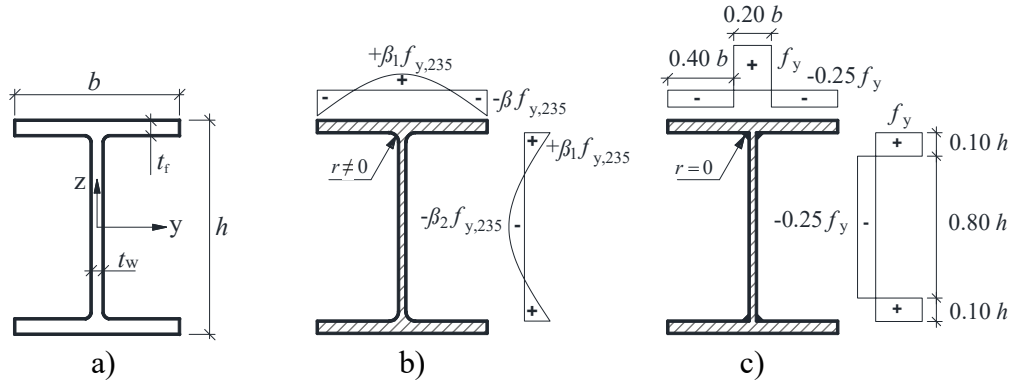


Figure 6: Residual stresses patterns – a) Section dimension – b) Hot-rolled I-sections – c) Welded I-sections.

Table 1: Magnitude of the residual stresses adopted in the numerical models.

	Hot-rolled sections (Fig. 6b)	Welded sections (Fig. 6c)
Type 1	$\min\{235 \text{ MPa}; f_{p,\theta}\}$	$f_{p,\theta}$
Type 2	$\min\{235 \text{ MPa}; f_{y,\theta}\}$	$f_{y,\theta}$

2.2 Validation of F.E. models

To validate the F.E. models, the ultimate resistances, deformation shapes and load displacement curves derived from numerical models were compared to their experimental counterparts [(Pauli, 2013), (Hricak et al., 2014)]. A total of 16 specimens have been considered, including (i) 12 hot-rolled HEA100 stub columns at 400 °C, 550 °C and 700 °C and at a strain rate of 0.10 %/min and (ii) 4 welded section beams at 450 °C and 650 °C. The measured geometrical dimensions, material properties, initial imperfections, and load eccentricities have been considered in numerical models. Besides, a sensitivity analysis was performed to examine the influence of (i) various geometrical imperfection amplitudes and (ii) two types of residual stresses on the ultimate resistance of I-sections in case of fire. The aim was to identify the most appropriate values to use in subsequent parametric studies. The comparisons between experimental $N_{u, Exp.}$ and corresponding numerical $N_{u, F.E.}$ results are summarized in Table 2, where the numerical predictions are on the safe side if $N_{u, F.E.} / N_{u, Exp.} < 1.0$ and vice versa.

Table 2: Comparison of experimental and numerical results with different magnitudes of the residual stresses and imperfection amplitudes.

Source	Specimen	Dimensions [mm] $h \times b \times t_f \times t_w$	L [mm]	$f_{y,20^\circ\text{C}}$ [MPa] web/flange	Loading	a_{measured} [mm] web/flange	T [°C]	$N_{u, \text{Exp.}}$ [kN]	$N_{u, \text{F.E.}} / N_{u, \text{Exp.}} [-]$				Type 2 ($f_{y,\theta}$)																							
									Type 1 ($f_{p,\theta}$)				a_{measured}	$a/200$																						
								a_{measured}	$a_i / 100$	$a_i / 200$	$a_i / 400$	a_{measured}	$a/200$																							
Hot-rolled sections (Pauli, 2013)	S01	96×100×5×8	300	425/425	N	0.20 / 0.20	400	996	0.95	0.90	0.93	0.95	0.95	0.93																						
	S02														$N+M_y - e_y = 10 \text{ mm}$	0.15 / 0.15	550	511	0.95	0.90	0.93	0.94	0.95	0.93												
	S03																								0.12 / 0.12	700	162	1.05	1.04	1.05	1.05	1.05	1.05			
	S04				0.29 / 0.29	400	764	0.94	0.91	0.93	0.94	0.94	0.93																							
	S05													0.09 / 0.09	550	389	0.96	0.94	0.95	0.96	0.96	0.95														
	S06																						0.12 / 0.12	400	467	0.91	0.88	0.90	0.91	0.91	0.90					
	S07				$N+M_y - e_y = 50 \text{ mm}$	0.13 / 0.13	550	225	0.98	0.95	0.97	0.98	0.98																			0.97				
	S08													0.16 / 0.16	550	236	0.93	0.91	0.93	0.93	0.93	0.93														
	S09																						$N+M_z - e_z = 10 \text{ mm}$	0.15 / 0.15	400	739	0.86	0.85	0.86	0.86	0.86		0.86			
	S10				0.14 / 0.14	550	376	0.92	0.91	0.91	0.92	0.92	0.91																							
	S11													$N+M_z - e_z = 50 \text{ mm}$	0.09 / 0.09	400	288	0.94	0.93	0.93	0.94	0.94										0.93				
	S12																						0.12 / 0.12	550	140	1.05	1.05	1.06	1.06	1.06	1.06					
Welded sections (Hricak et al., 2014)	S21	680×250×4×12	1500	393/427	M_y	4.77 / 1.20	450	638	0.91	0.89	0.91	0.93	0.92																				0.92			
	S22													846×300×8×8	382/340	1.34 / 1.98	650	231	0.95	0.94	0.95	0.95										0.95		0.95	0.95	
	S23																						2.36 / 1.92	450	485	1.07	1.06	1.07	1.07	1.07	1.07					1.07
	S24																																			
Mean		0.96	0.94	0.95	0.96	0.96	0.95																													
C.O.V.		0.06	0.07	0.06	0.06	0.06	0.06																													

In general, the comparison of experimental and numerical results reveals that the magnitude of the residual stresses and the amplitude of geometrical imperfection have a limited influence on the ultimate resistance of hot-rolled and welded I-sections at elevated temperatures. When considering Type 1 residual stresses patterns paired with measured maximum amplitudes $a_{measured}$, the numerical models were found to provide the closest predictions to experimental results – the corresponding mean value of the $N_{u,FE} / N_{u,exp.}$ ratio is 0.96, associated with a Coefficient of Variation (C.o.V.) as low as 0.06.

However, since obtaining measured or real amplitudes of imperfections in each member is practically impossible in practice, alternative “standard” definitions for such distributions of geometrical imperfections (both shapes and amplitudes) are necessary (Gérard et al., 2019). Accordingly, sine-based distributions of the local geometrical imperfection coupled were also tested, where amplitudes were chosen as fractions of plate buckling lengths a_i 's. As presented in Table 2, slightly less accurate results were obtained when using $a_i / 100$, with the lowest mean value of $N_{u,FE} / N_{u,exp.}$ (0.94) and the maximum C.o.V. (0.07). When considering amplitudes based on $a_i / 200$ values, which is in accordance with the suggestion in EN 1993-1-5 (European Committee for Standardisation, 2006) and in (Gérard et al., 2019), an average $N_{u,FE} / N_{u,exp.}$ ratio equal to 0.95 with a 0.06 C.o.V. are reported – these results are nearly as good as with considering $a_{measured}$. Therefore, sine-shaped local imperfections with amplitudes set as $a_i / 200$ were finally adopted in the F.E. models. It is worth noting that the influence of imperfections in fire conditions may be smaller when steel members are not subjected to high utilization ratios (Couto & Real, 2021), thus the proposed approach is conservative.

Besides, for F.E. models considering identical initial geometrical imperfections' amplitudes, equal $N_{u,FE} / N_{u,exp.}$ ratios mean and C.o.V. values are reported for the two possible magnitudes of the residual stresses, evidencing that the magnitude of the residual stresses has a negligible impact on the ultimate resistance of I-sections in fire. Hence, only the results with $a_{measured}$ and $a_i / 200$ are presented in Table 2. However, when using $f_{y,\theta}$ as a basis for the residual stresses' magnitude, some G.M.N.I.A. simulations showed certain stress redistributions during the initial, still elastic loading steps. Therefore, the proportional limit stress $f_{p,\theta}$ was finally selected as a basis for the magnitude of residual stresses in further parametric studies (i.e., “Type 1” definitions were adopted).

Figs. 7 and 8 further compare numerical and experimental load-displacement curves, as well as deformation shapes, where relatively good agreement is observed with respect to initial stiffness, peak loads, failure modes and the general shape of load-displacement curves. Overall, given the many uncertainties in performing structural fire tests and the complex buckling behavior of cross-sections at elevated temperatures, the numerical models are evidenced to be suitable and accurate for predicting fire cross-section resistances and therefore have been used extensively within extensive numerical parametric studies.

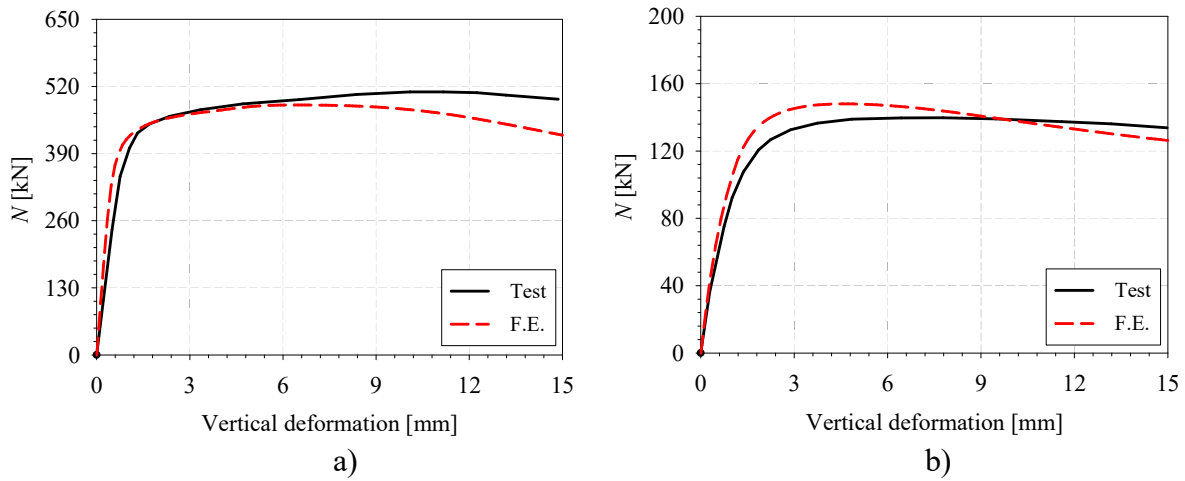


Figure 7: Comparison of numerical and experimental load-displacement curves for specimen – a) S02 – b) S12.

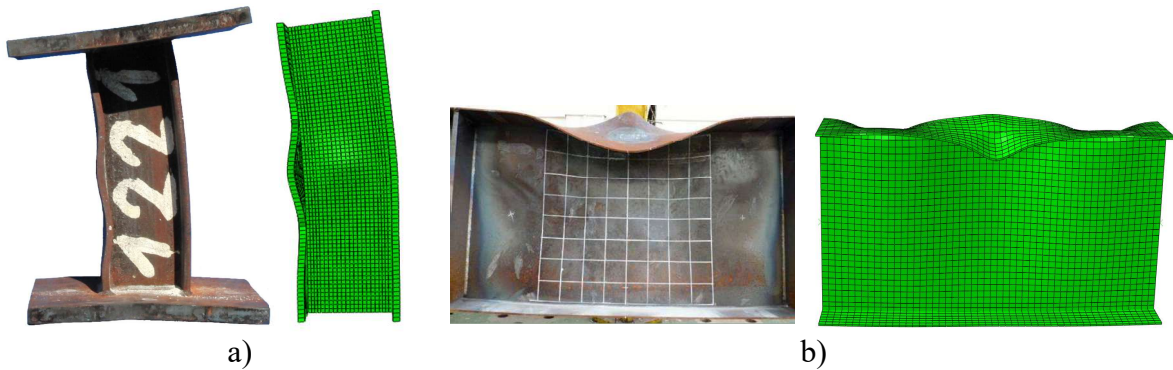


Figure 8: Comparison between numerical and experimental deformation shapes for specimen – a) S02 – b) S24.

Some 3 852 G.M.N.I.A. simulations, including 54 hot-rolled and 53 welded sections, have been performed for I-sections at elevated temperatures. These selected section geometries spanned from plastic (Class 1) to slender (Class 4) sections, defined in accordance with the slenderness limits provided in Eurocode 3 (European Committee for Standardisation, 2007), (European Committee for Standardisation, 2005). The h / b aspect ratio of hot-rolled sections varied between 0.95 and 3.36, with $b / (2 t_f)$ spanning from 2.5 to 10.0 and h / t_w from 4.4 to 45.5. In contrast, more diverse and slender section geometries have been considered for welded sections: the aspect ratio h / b varied between 0.79 and 3.34, with $b / (2 t_f)$ spanning from 3.3 to 20.3 and h / t_w from 12.3 to 78.6. Note that the heights, widths and thickness were in all cases carefully chosen so as to be well proportioned. For each section shape, several parameters have been varied as follows: (i) three simple loading situations – axial compression N , major-axis bending M_y and minor-axis bending M_z , (ii) four fire temperatures – 350 °C, 450 °C, 550 °C, 700 °C and (iii) three steel grades – S355 steel with $f_y = 355$ MPa, S460 with $f_y = 460$ MPa, and S690 with $f_y = 690$ MPa. The latter one was considered for hot-rolled sections in order to expand the application scope of the current study. Key observations and analyses on the obtained numerical results are described in the next paragraphs.

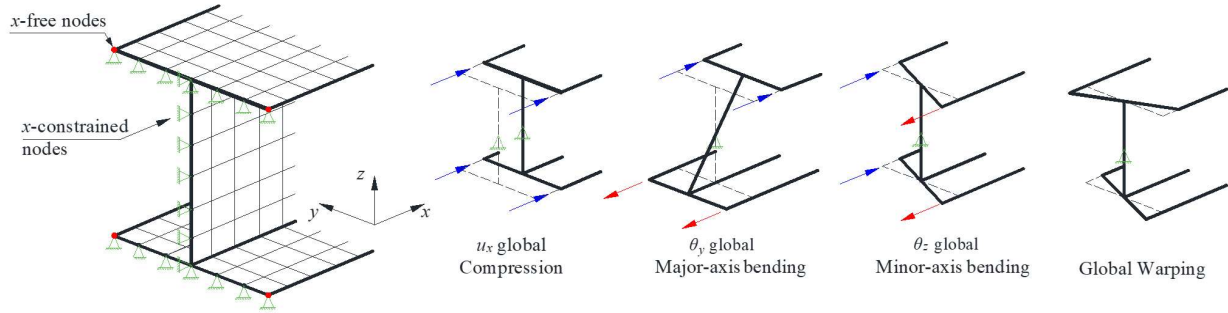


Figure 9: Boundary conditions and load application in parametric studies.

3.1 Evolution of cross-section resistance with increases in temperature

Fig. 10 presents all F.E. results in a so-called “O.I.C. general $\chi_L - \lambda_L$ format”, which allows displaying and comparing all cross-sections at various temperatures and under different loading situations. The horizontal axes in Fig. 10 represent the cross-section local relative slenderness λ_L and the vertical axes refer to the local buckling reduction factor χ_L (see definitions in Fig. 1). Note that for simple load cases, χ_L can also be expressed as $\chi_L = N_{u,F.E.} / (f_{y,\theta} \cdot A)$ for sections under compression N and $\chi_L = M_{u,F.E.} / (f_{y,\theta} \cdot W_{pl})$ for sections under M_y or M_z , where A is the gross section area, W_{pl} is the section’s plastic modulus, and $N_{u,F.E.}$ and $M_{u,F.E.}$ are the ultimate compression load and ultimate bending moment obtained numerically, respectively. Besides numerical results, a horizontal $\chi_L = 1.0$ segment (indicating plastic resistance) as well as Von Karman’s elastic plate buckling curve, i.e., $\chi_L = 1 / \lambda_L$, are also plotted in Fig. 10 as reference curves. In Fig. 10 and the next ones, it is possible to observe that although strain hardening effects were not considered in the numerical models, some values of χ_L can be slightly higher than 1.0 when it comes to very compact sections with low λ_L . this shall be attributed to the plasticity spreading in the longitudinal direction, which gives the “stub columns” or short members a little extra resistance prior to collapse. This phenomenon cannot be deemed to be representative of cross-sectional behaviour and is also known to disappear completely when considering member resistance (Hayeck, 2016). Accordingly, the maximum reduction factor considered in the O.I.C. design equations detailed in Section 4 have been limited to $\chi_L = 1.0$.

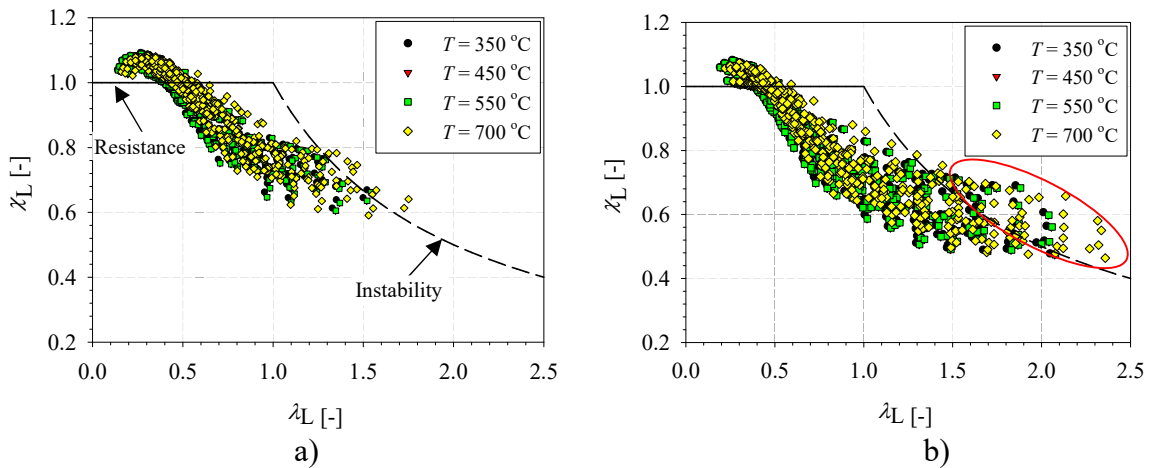


Figure 10: Influence of temperature on section resistance considering all yield strengths and all load cases – a) Hot-rolled sections – b) Welded sections.

Besides that, other tendencies are observed. Since more diverse and more slender section shapes have been considered for welded I-sections, the results presented in Fig. 10b seem more scattered than the results presented in Fig. 10a for hot-rolled I-sections. λ_L is indeed seen to reach values up to 2.4 for welded sections but lower than 1.8 for hot-rolled sections. For some very slender welded I-sections (see red ellipse), apparent post-buckling effects can be observed. For a given section geometry and at room temperature, hot-rolled I-sections usually attain higher cross-section resistance, owing to more favourable residual stresses patterns than in welded I-sections (Gérard et al., 2021). However, residual stresses become less influential when temperature increases, so closer results are reported in Fig. 10 between hot-rolled and welded sections.

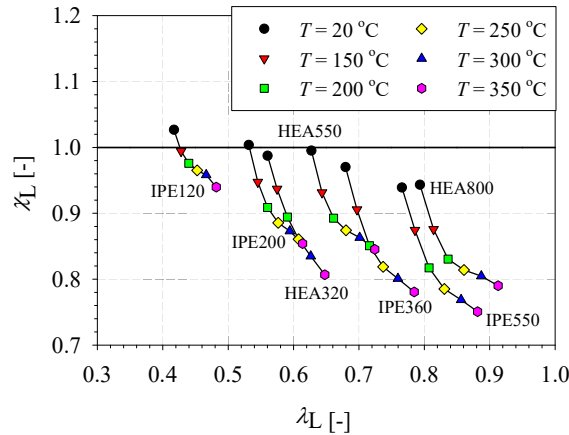


Figure 11: Evolution of resistance with an increase in temperature from 20 °C to 350 °C for various hot-rolled sections under compression N .

Fig. 10b also shows that increases in temperature do not change the trends observed, since the influence of material properties – including Young's modulus and effective yield stress which decrease with temperature – have been sufficiently accounted for through the O.I.C. format, i.e., within the definitions of λ_L and χ_L . However, compared to the results reported in (Gérard et al., 2021) for I-sections at ambient temperature, quite lower relative resistances χ_L can be achieved. Accordingly, a specific sub-study was carried out to analyze the evolution of section resistance within lower temperature ranges for six hot-rolled I-sections under axial compression N with the steel grade S355. As shown in Fig. 11, when temperature increases from 20 °C to 350 °C, all relative resistances χ_L decrease rapidly with limited increases in λ_L ; in particular, the drop in χ_L is more severe for slender sections than for compact sections. From 20 °C to 350 °C, ratios of $k_{p,\theta} / k_{y,\theta}$ decline drastically (see Fig. 4b), since the linear portion of the stress-strain relationship reduces continuously with increases in temperature. Accordingly, this more pronounced non-linear material response further accelerates local buckling. In addition, given the inverse relationship between cross-section slenderness λ_L and $(k_{E,\theta} / k_{y,\theta})^{0.5}$, cf. Fig. 4, the values of λ_L rise up steadily with increases in temperatures in Fig. 11. In contrast, the influence of high temperatures on the results presented in Fig. 10 is seen to be of lesser importance owing to the values of $k_{p,\theta} / k_{y,\theta}$ and $(k_{E,\theta} / k_{y,\theta})^{0.5}$ changing at the same rate beyond 400 °C. On the other hand, these ranges of temperature are below those that are relevant for practical situations (Maia et al., 2016).

Finally, as shown in Fig. 11, all section shapes do not exhibit identical trends, indicating that section geometry has an impact on local buckling behavior at different temperatures. In general, although lower section resistances χ_L are reported when considering higher temperatures, similar tendencies are observed for sections at 20 °C and at temperatures higher than 350 °C. Therefore, the behavior of I-sections at elevated temperatures can be seen as an extension from that at room temperatures.

3.2 Influence of load case on section resistance

Fig. 12 displays numerical results for sections at 550 °C under different simple loading cases, i.e., axial compression N , major-axis bending M_y or minor-axis bending M_z , respectively.

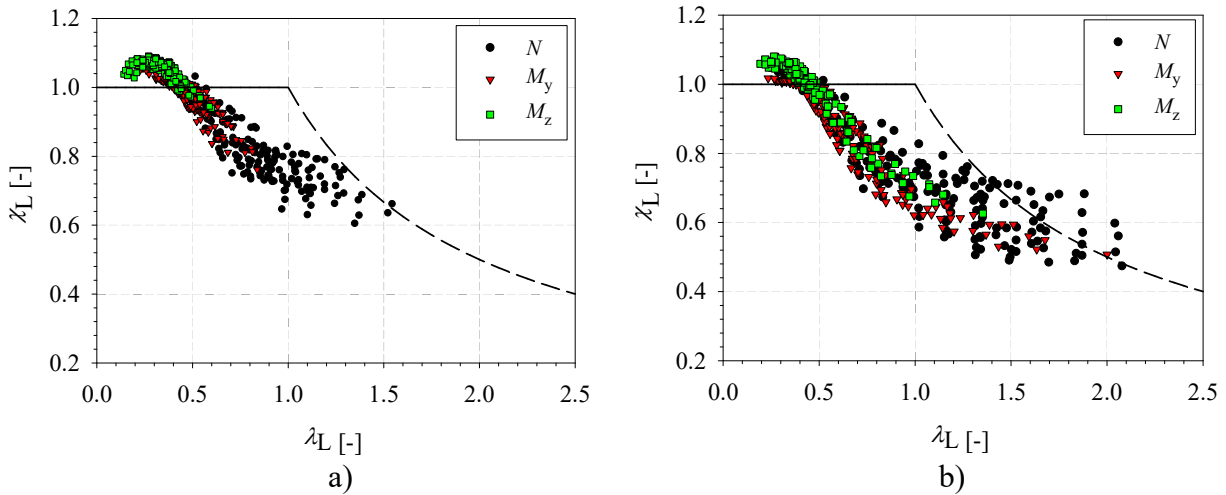


Figure 12: Influence of load case on section resistance at 550 °C – a) Hot-rolled sections – b) Welded sections.

It can be observed that:

- The slenderness range for λ_L values in hot-rolled sections varies considerably with the different load cases – λ_L can reach up to 1.5 for sections under N but only roughly 0.9 for sections under M_y and about 0.6 for sections under M_z . Most of hot-rolled sections in usual catalogues [(American Institute of Steel Construction, 2017), (British Constructional Steelwork Association, 2013)] considered here usually have non-slender flanges but relatively more slender webs. Therefore, losses in cross-sectional strength are mainly due to local buckling in the web plates under compression stresses, while for M_y and M_z load cases, where local buckling is prone to occur in flange plates, the range of section slenderness λ_L shall be more limited than for compression cases. In contrast, λ_L ranges for welded sections remain wider, since more slender section shapes including some with slender flange plates have been considered in this paper – λ_L can reach up to 2.0 for sections under M_y which is very close to the maximum λ_L for compression load cases. Besides, the lower bounds of the χ_L values in Fig. 12b are close among different load cases, which is similar to the results obtained from I-sections at ambient temperatures [(Gérard et al., 2021), (Li et al., 2022)];
- The results presented in Fig. 12 indicate that, except for M_y and M_z load cases, where the results are less scattered, proposing a single, safe-sided design curve would be too conservative and uneconomical, especially for compression load cases. In this respect, further analyses have been carried out, such as in previous studies [(Gérard et al., 2021),

(Li et al., 2022b), (Li et al., 2022c)], to characterize the influence of section geometries on cross-section resistance at ambient temperatures, and two geometrical parameters γ_{HR} and γ_W have been proposed to capture the observed scatters. Further discussion on the proposed design approach is provided in next Section 4.

3.3 Influence of steel grade on section resistance

Fig. 13 presents the numerical results obtained for I-sections under axial compression N concerning three different steel grades, i.e., S355, S460 and S690 steel. Compared to the results in (Li et al., 2022), the influence of steel grades on cross-section resistance at elevated temperatures is more noticeable than that at room temperature. For both hot-rolled and welded I-sections, higher steel grades can offer greater nominal section resistance with a given χ_L value. In particular for the results with $\lambda_L = 0.7$, the maximum difference can reach around 10%. However, since the change in steel grades only affects the general trends of the results on a limited scale, the O.I.C.-based design formulae proposed in Section 4 were built based on the safe-side results with S355 steel grade.

4 O.I.C. design curves

Based on the F.E. results collected along the parametric studies, design provisions for I-sections in fire have been formulated, following the O.I.C framework (see Fig. 1). The O.I.C. general $\chi_L - \chi_L$ format was developed based on the well-known Ayrton-Perry approach [(Ayrton & Perry, 1886), (Maquoi & Rondal, 1978)], which has been adopted in Eurocode 3 (European Committee for Standardisation, 2005) as member buckling curves for decades. For cross-section resistance without considering strain hardening effects, the relationship between local buckling reduction factor χ_L and local relative slenderness λ_L is defined by Eqs. (3) and (4), where λ_0 represents the length of a resistance plateau, for which $\chi_L = 1.0$, α_L is a generalised imperfection factor and δ further considers post-buckling effects.

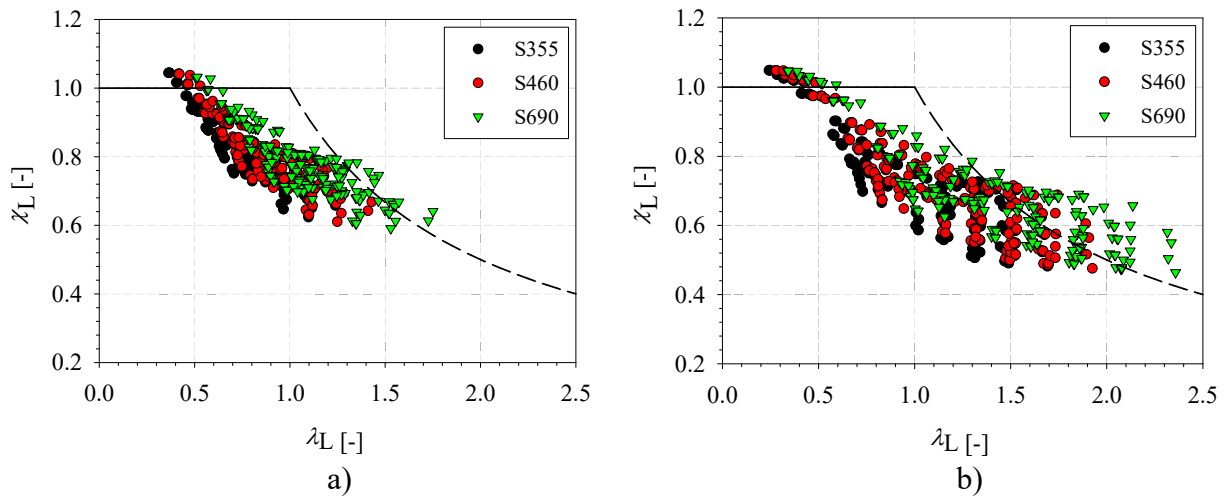


Figure 13: Influence of steel grade on the resistance of I-sections under N – a) Hot-rolled sections – b) Welded sections.

$$\chi_L = \frac{1}{\phi_L + \sqrt{\phi_L^2 - \bar{\lambda}_L^\delta}} \quad (3)$$

$$\phi_L = 0.5 \cdot \left(1 + \alpha_L \cdot (\bar{\lambda}_L - \lambda_0) + \bar{\lambda}_L^\delta\right) \quad (4)$$

As discussed in Section 3.2, relying on a single, safe-sided design curve is deemed too conservative and uneconomical, especially for compression load cases. Therefore, in order to accommodate the scattered results as shown in Fig. 12, a series of parametric buckling curves is proposed by adjusting the values of α_L and δ through geometrical parameters γ denoted γ_{HR} for hot-rolled profiles and γ_W for welded ones as defined by Eqs. (3) and (4), i.e., $\alpha_L = f^\circ(\gamma)$ and $\delta = f^\circ(\gamma)$. Since most of the hot-rolled sections in usual catalogues [(American Institute of Steel Construction, 2017), (British Constructional Steelwork Association, 2013)] comprise non-slender flanges while welded I-sections bear more diverse geometries in addition to different manufacturing processes, two different γ factors, i.e., γ_{HR} and γ_W , have been considered. As discussed in Section 3.1, the influence of section geometries on cross-section resistance at temperatures greater than 350 °C and at 20 °C being similar, parameters γ_{HR} and γ_W proposed for I-sections at ambient temperatures [(Gérard et al., 2021), (Li et al., 2022)] are adopted as well for fire situations.

Eqs. (1) to (4) together with Table 3 summarize the proposed approach to predicting the ultimate resistance of I-sections under three simple loading cases at elevated temperatures (from 350 °C to 700 °C). A sample of results on all I-sections under compression N with three γ lower bounds of design curves is proposed in Fig. 14.

$$\gamma_{HR} = \frac{b}{t_f} \cdot \left(\frac{h}{t_w}\right)^2 \cdot \frac{t_w}{t_f} \cdot 10^{-5} \quad (5)$$

$$\gamma_W = \frac{b}{h} \cdot \frac{t_w}{t_f} \quad (6)$$

Table 3: O.I.C.-based design proposal for hot-rolled and welded sections.

Load cases	Hot-rolled I-sections	Welded I-sections
Compression N	$\lambda_0 = 0.4$ $\alpha_L = 1.4$ $\delta = -1.3 \cdot \gamma_{HR} + 0.2$	$\lambda_0 = 0.4$ $\alpha_L = 0.85 \cdot \gamma_W$ $\delta = \gamma_W$
Major-axis bending M_y	$\lambda_0 = 0.4$ $\alpha_L = 0.2$ $\delta = 0.5$	$\lambda_0 = 0.4$ $\alpha_L = 0.35$ $\delta = 0.2$
Minor-axis bending M_z	$\lambda_0 = 0.4$ $\alpha_L = 0.1$ $\delta = 0.2$	$\lambda_0 = 0.4$ $\alpha_L = 0.25$ $\delta = 0.5$

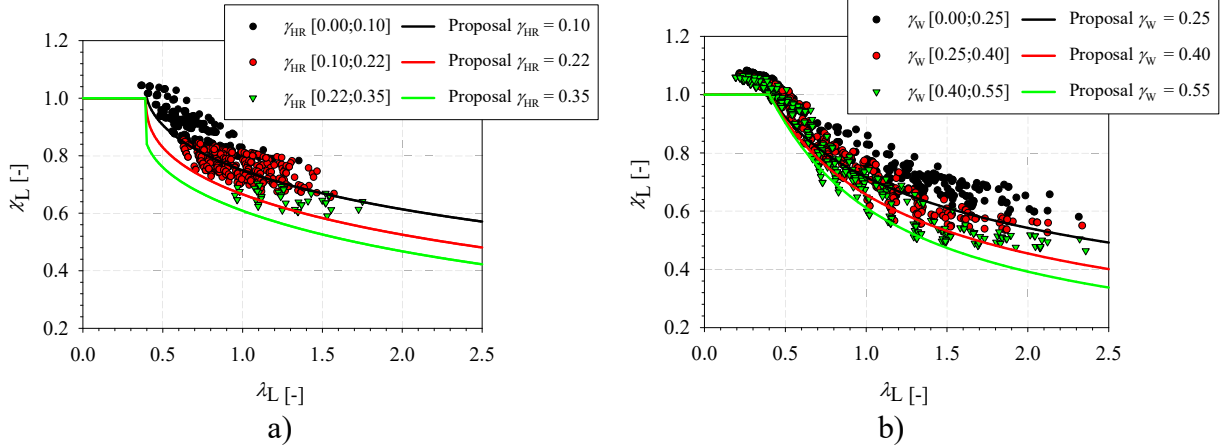


Figure 14: Section resistance under compression N and γ parameters – a) Hot-rolled sections – b) Welded sections.

5 Accuracy of design rules

In this section, the accuracy of resistance predictions from existing European Standard EN 1993-1-2 (EC 3) (European Committee for Standardisation, 2007), upcoming standard prEN 1993-1-2 (prEC 3) (European Committee for Standardisation, 2020) and the proposed O.I.C. design approach is assessed. Note that this paper only focuses the local buckling behaviour of steel I-sections in fire, so the reduction factor as defined in [(European Committee for Standardisation, 2007), (European Committee for Standardisation, 2020)] for member buckling in the fire design situation were not applied. Figs. 15a to 20a plot $\chi_{L,Ref.} / \chi_{L,F.E.}$ ratios as a function of cross-section local slenderness λ_L , where $\chi_{L,F.E.}$ represents the numerical results and $\chi_{L,Ref.}$ refers to the ultimate resistance predicted by one of the three reference design rules, i.e., $\chi_{L,EC 3}$, $\chi_{L,prEC 3}$ and $\chi_{L,O.I.C.}$. If $\chi_{L,Ref.} / \chi_{L,F.E.}$ is lower than 1.0, the analytical prediction remains on the safe side, and vice-versa. Figs. 15b to 20b plot the corresponding frequency histograms as a complement, allowing for an overall statistical analysis of the results. Tables 4 to 6 also reports key statistical results on the $\chi_{L,Ref.} / \chi_{L,F.E.}$ ratios, including the mean values, C.o.V.s, maximum and minimum values, and the proportions of results larger than 1.0 and 1.15 on the unsafe side.

5.1 Resistance to axial compression

As shown in Figs. 15 and 16 and Table 4, the design rules given in both EC 3 and in the upcoming prEC 3 lead to significant inaccurate and scattered predictions for hot-rolled and welded sections under axial compression. Mean values of the $\chi_{L,EC 3} / \chi_{L,F.E.}$ ratios are 0.85 with a C.o.V. higher than 0.13. For semi-compact sections (or Class 3 sections, with intermediate local slenderness i.e., $\chi_L \approx [0.50-0.70]$), the EC 3 predictions are generally on the unsafe side, resulting in 4.6% of the results for hot-rolled sections and 1.3% of the results for welded sections being over 1.15 on the unsafe side. Moreover, since EC 3 considers the effective yield strength $f_{p,\theta}$ to calculate the resistance of non-slender (Class 1-3) sections, but 0.2% proof strength $f_{p0.2,\theta}$ for slender (Class 4) sections (see Fig. 4), obvious discontinuities in $\chi_{L,EC 3} / \chi_{L,F.E.}$ ratios are observed when λ_L is around 0.7. In comparison, more unsafe results are predicted by prEC 3 for semi-compact sections. For hot-rolled sections, the mean value of $\chi_{L,prEC 3} / \chi_{L,F.E.}$ is 1.06 and more than 78% of the predictions are unsafe, among which 11.1% lie beyond 15% on the unsafe side. Note that both EC 3 and prEC 3 determine the limits of width-to-thickness ratios by using the material factor ε_θ as defined in Eq. (5), where 0.85 is a mean value of the $(k_{E,\theta}/k_{y,\theta})^{0.5}$ ratio, as shown in Fig. 4. For sections at

700 °C, where the $(k_{E,\theta}/k_{y,\theta})^{0.5}$ ratio is lower than 0.85, the material factor ε_θ as well as limits of width-to-thickness ratios are overestimated. Consequently, many EC 3 and prEC 3 resistance predictions for sections at 700 °C are on the unsafe side, although it should be mentioned that these unsafe results, particularly for Class 4 sections, are then compensated by the use of a reduction factor for the flexural buckling for the design of axial compressed members, which then results in an acceptable safety margin for their design (Couto et al., 2016). Also, in particular for the steel grades of S690 the limited studies, on the subject seems to suggest that improved design proposals may be still necessary to proper account with local buckling [(Kucukler, 2021), (Couto & Real, 2019)].

$$\varepsilon_\theta = \sqrt{k_{E,\theta}/k_{y,\theta}} \cdot \sqrt{235/f_y} \approx 0.85\sqrt{235/f_y} \quad (7)$$

In contrast, the O.I.C. proposal performs better than the EC 3 and prEC 3 design rules for both hot-rolled and welded I-sections. As shown in Figs. 15b and 16b, the O.I.C. provides more consistent and less scattered predictions than EC 3 and prEC 3 ones. In addition, Table 4 reports key statistical data where mean values of the $\chi_{L,O.I.C.} / \chi_{L,F.E.}$ ratio are seen to remain above 0.94 with C.o.V. values as low as 0.06, combined with more than 86% of predictions lying on the safe side; also, no O.I.C. prediction larger than 1.15 (i.e., 15% on the unsafe side) is reported. Besides, the minimum value of $\chi_{L,O.I.C.} / \chi_{L,F.E.}$ remains 0.79 for hot-rolled sections and 0.75 for welded sections, respectively, which are higher values than for EC 3 predictions, whose $\chi_{L,EC3} / \chi_{L,F.E.}$ ratios may reach values as low as 0.59.

5.2 Resistance to major-axis bending

Results for steel sections in fire subjected to major-axis bending are reported in Fig. 17 and 18, as well as in Table 5. Similar to the compression load case, both EC 3 and prEC 3 generally provide more scattered and unsafe resistance predictions than the O.I.C.-based proposal for sections under major-axis bending M_y . Since EC 3 considers different design strengths for non-slender and slender sections, the results in Figs. 17 and 18 exhibit notable inconsistencies for λ_L around 0.7 to 0.9, leading to higher C.o.V. values. Although prEC 3 provides more continuous predictions, it still results in a higher proportion of unsafe outcomes. For hot-rolled sections under M_y where most sections have relatively compact flanges and semi-compact webs, 57.9% of the prEC 3 predictions remain on the unsafe side. As for welded sections – recall that more slender sections have been considered –, 46.7% of the results are unsafe. In fact, in (Couto et al., 2015) it was demonstrated that an effective section might be necessary for Class 3 sections, and in (Couto et al. 2014) that local buckling could also reduce the section resistance of more compact sections within the Class 1 and 2 limits, which explains the obtained results.

In comparison, the O.I.C. brings more accurate resistance predictions and a smooth continuity from compact to slender sections is observed. For hot-rolled sections, less than 15.6% of all $\chi_{L,O.I.C.} / \chi_{L,F.E.}$ ratios are on the unsafe side with an extremely low C.o.V. equal to 0.03. For welded sections, the O.I.C. predictions never exceed 4% of over-conservatism with a minimum value equaling to 0.80, which is higher than the minimum values derived from EC 3 and prEC 3.

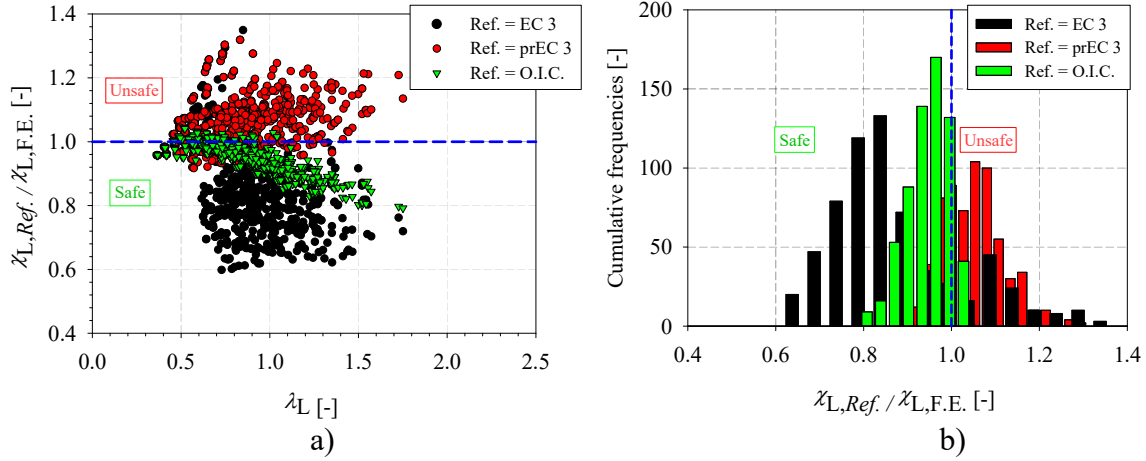


Figure 15: Design rules vs. numerical results for hot-rolled sections under compression N – a) Accuracy of resistance predictions as a function of λ_L – b) Frequency distributions.

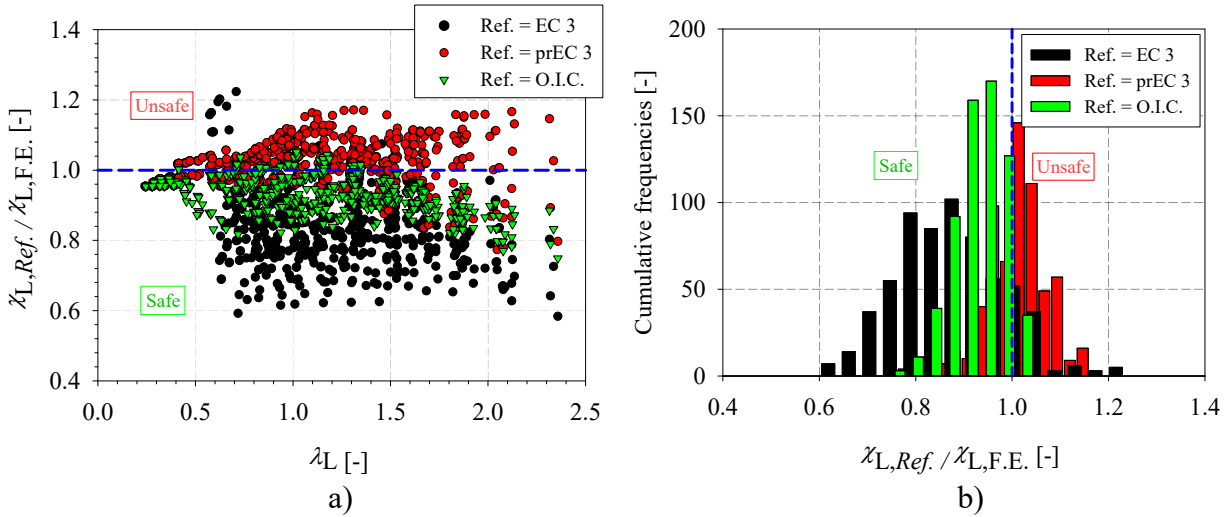


Figure 16: Design rules vs. numerical results for welded sections under compression N – a) Accuracy of resistance predictions as a function of λ_L – b) Frequency distributions.

Table 4: Statistical analysis of $\chi_{L,Ref.} / \chi_{L,F.E.}$ ratios for sections under compression N .

	Proposal	Mean	C.o.V.	Max.	Min.	>1.0 [%]	>1.15 [%]
Hot-rolled sections	O.I.C.	0.95	0.05	1.04	0.79	14.0	0.0
	EC 3	0.85	0.17	1.35	0.60	17.9	4.6
	prEC 3	1.06	0.07	1.32	0.92	78.2	11.1
Welded sections	O.I.C.	0.94	0.06	1.05	0.75	10.5	0.0
	EC 3	0.85	0.13	1.22	0.58	9.3	1.3
	prEC 3	1.02	0.06	1.17	0.77	66.2	2.2

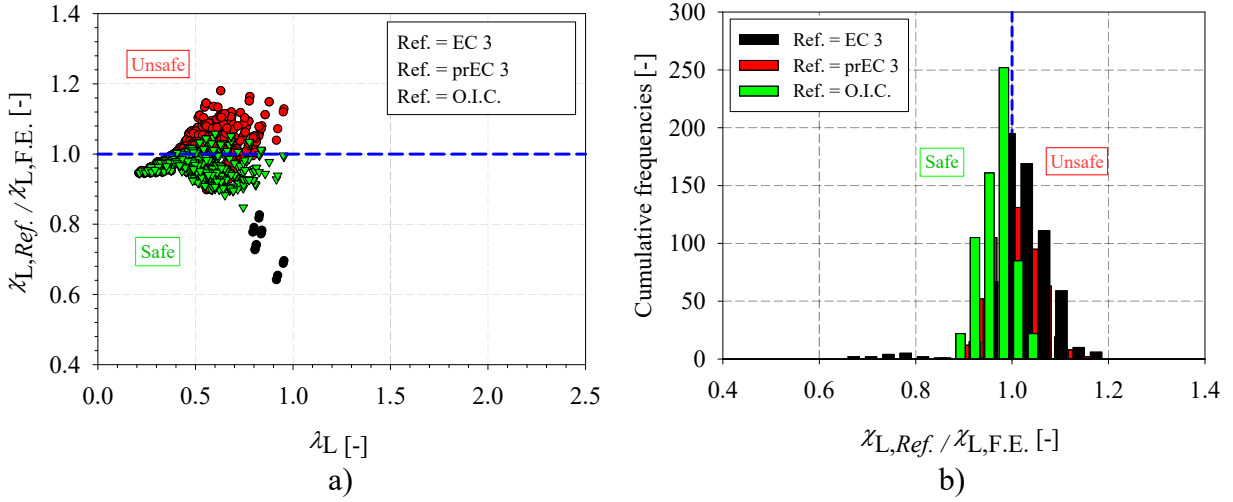


Figure 17: Design rules vs. numerical results for hot-rolled sections under major-axis bending moment M_y – a) Accuracy of resistance predictions as a function of λ_L – b) Frequency distributions.

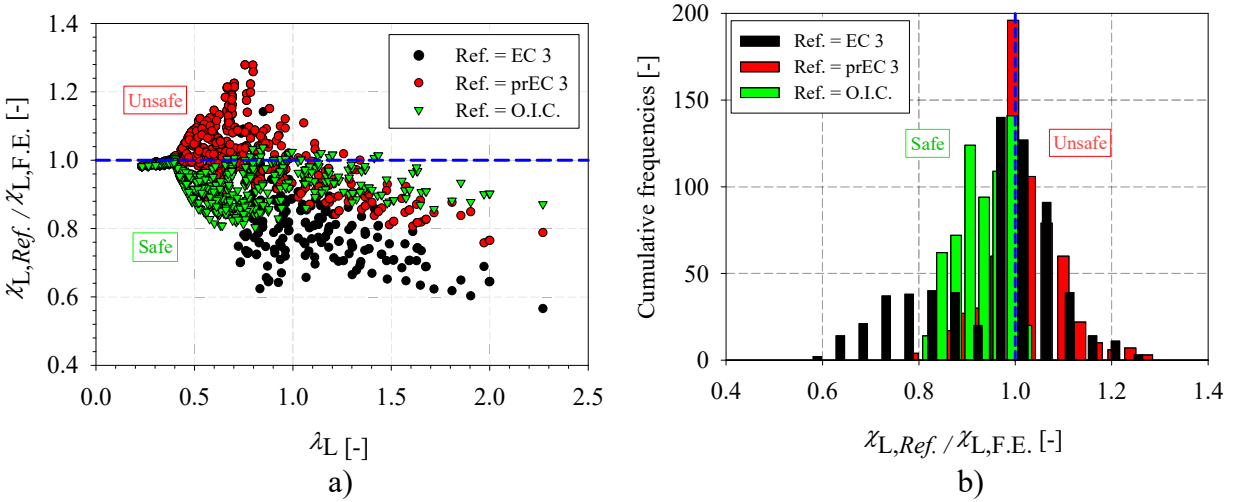


Figure 18: Design rules vs. numerical results for welded sections under major-axis bending moment M_y – a) Accuracy of resistance predictions as a function of λ_L – b) Frequency distributions.

Table 5: Statistical analysis of $\chi_{L,Ref.} / \chi_{L,F.E.}$ ratios for sections major-axis bending moment M_y .

	Proposal	Mean	C.o.V.	Max.	Min.	>1.0 [%]	>1.15 [%]
Hot-rolled sections	O.I.C.	0.97	0.03	1.06	0.85	15.6	0.0
	EC 3	1.01	0.06	1.18	0.64	55.6	0.5
	prEC 3	1.01	0.05	1.18	0.90	57.9	0.5
Welded sections	O.I.C.	0.93	0.05	1.04	0.80	6.3	0.0
	EC 3	0.95	0.14	1.28	0.57	39.6	3.6
	prEC 3	1.00	0.08	1.28	0.76	46.7	3.6

5.3 Resistance to minor-axis bending

This subsection compares various fire design rules with the reference numerical results for I-sections under minor-axis bending; results are presented in Figs. 19 and 20, complemented by Table 6. Predictions from EC 3 design requirements again exhibit two obvious discontinuities. For $\lambda_L \approx 0.4$, corresponding to the relative slenderness limit between Class 2 to Class 3 sections per EC 3, the average value of $\chi_{L,EC3} / \chi_{L,F.E.}$ suddenly drops from 0.95 to 0.7, leading to overly conservative resistance estimates beyond this limit (see the impact on accuracy and frequency distributions, identified in blue rectangles in Figs. 19 and 20). Here again, EC 3 allowing for plastic capacities for Class 2 sections but limiting to elastic capacities for Class 3 sections yields inaccurate predictions.

The second discontinuity occurs around $\lambda_L \approx 0.6$, as a consequence of EC 3 abruptly reducing the design yield strength from $f_{y,\theta}$ to $f_{p0.2,\theta}$, resulting in an average $\chi_{L,EC3} / \chi_{L,F.E.}$ ratio for Class 4 sections as low as 0.5 (see purple rectangle in Fig. 20). In some cases, minimum values may even drop below 0.4, meaning that the “true” resistance is substantially higher than the code’s prediction. In comparison, prEC 3 yields more accurate results, as it uses an identical design yield strength related to $f_{y,\theta}$ for Class 1 to Class 4 sections.

In contrast, the O.I.C.-based approach provides the best resistance predictions, with mean values close to 1.0 as well as the lowest C.o.V. values which are remarkably low at 0.02. Besides, the minimum values of $\chi_{L,O.I.C.} / \chi_{L,F.E.}$ exceed 0.89, which are much higher than its EC 3 counterparts. Overall, given the wide range of section dimensions and the complex cross-sectional behavior at elevated temperatures, the O.I.C. proposal is proved to be an adequate and reliable design approach.

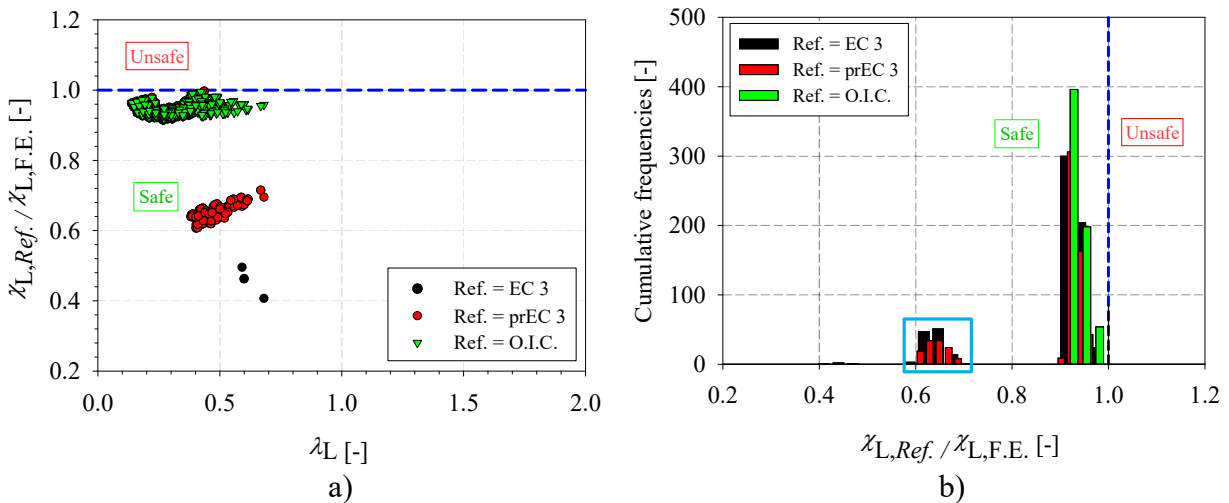


Figure 19: Design rules vs. numerical results for hot-rolled sections under minor-axis bending moment M_z – a) Accuracy of resistance predictions as a function of λ_L – b) Frequency distributions.

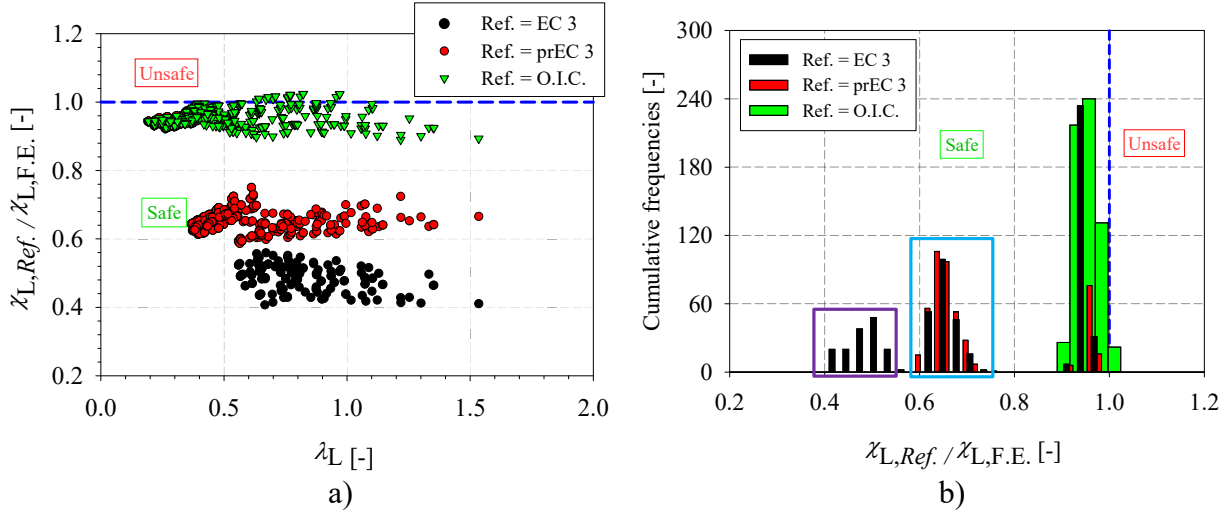


Figure 20: Design rules vs. numerical results for hot-rolled sections under minor-axis bending moment M_z – a) Accuracy of resistance predictions as a function of λ_L – b) Frequency distributions.

Table 6: Statistical analysis of $\chi_{L,Ref.} / \chi_{L,F.E.}$ ratios for sections minor-axis bending moment M_z .

	Proposal	Mean	C.o.V.	Max.	Min.	>1.0 [%]	>1.15 [%]
Hot-rolled sections	O.I.C.	0.94	0.02	1.00	0.92	0.0	0.0
	EC 3	0.88	0.13	1.00	0.41	0.0	0.0
	prEC 3	0.89	0.13	1.00	0.61	0.0	0.0
Welded sections	O.I.C.	0.95	0.02	1.02	0.89	3.3	0.0
	EC 3	0.74	0.26	0.99	0.41	0.0	0.0
	prEC 3	0.78	0.19	0.99	0.59	0.0	0.0

5.4 Reliability analyses

The reliability levels of the three analytical proposals for hot-rolled and welded I-sections under simple load cases in the case of fire may be assessed through the 3 criteria suggested by Kruppa (Kruppa, 1999); the latter can be summarized as follows:

- I. No $\chi_{L,Ref.} / \chi_{L,F.E.}$ ratio shall be on the unsafe side by more than 15% (i.e., $\chi_{L,Ref.} / \chi_{L,F.E.} \leq 1.15$);
- II. The proportion of unsafe predictions ($\chi_{L,Ref.} / \chi_{L,F.E.} > 1.0$) shall be less than 20%;
- III. The mean value of all $\chi_{L,Ref.} / \chi_{L,F.E.}$ ratios shall be on the safe side.

Based on the statistical analyses presented in Tables 4 to 6, the reliability assessment results are summarized in Table 7 for the three fire design approaches considered in this paper. It is evident that the EC 3 and prEC 3 predictions often violate Kruppa's criteria except for the I-sections under minor-axis bending. In comparison, the O.I.C.-based approach fulfills all three Kruppa's criteria and hence is capable of providing reliable predictions for the ultimate resistance of hot-rolled and welded I-sections at elevated temperatures from 350 °C to 700 °C.

Table 7: Results of reliability analyses according to Kruppa’s criteria (Kruppa, 1999).

Load cases	Criteria #	Hot-rolled I-sections			Welded I-sections		
		O.I.C.	EC 3	prEC 3	O.I.C.	EC 3	prEC 3
N	I	✓	✗	✗	✓	✗	✗
	II	✓	✓	✗	✓	✓	✗
	III	✓	✓	✗	✓	✓	✗
M_y	I	✓	✗	✗	✓	✗	✗
	II	✓	✗	✗	✓	✗	✗
	III	✓	✗	✗	✓	✓	✓
M_z	I	✓	✓	✓	✓	✓	✓
	II	✓	✓	✓	✓	✓	✓
	III	✓	✓	✓	✓	✓	✓

6 Conclusions and future developments

This paper investigated numerically the local buckling behavior of hot-rolled and welded I-sections at elevated temperatures from 350 °C to 700 °C. Three simple load cases, i.e., axial compression N , major-axis bending M_y and minor-axis bending M_z have been considered. After developing and rigorously validating advanced non-linear shell models against steady-state experimental results, a series of parametric studies have been carried out to characterize the structural performance of I-sections where various section geometries, cross-section slenderness, yield limits and fire temperatures were considered.

The numerical results were then used to assess the performance of existing standard EN 1993-1-2 (EC 3) and its upcoming revision prEN 1993-1-2 (prEC 3). It was found that these two sets of design rules provide inaccurate and scattered resistance predictions for hot-rolled and welded I-sections in fire. Especially for Class 3 I-sections under N or M_y , where large proportions of unsafe results were observed. Besides, cross-section capacities predicted by EC 3 exhibited important resistance discontinuities around the Class 2-3 and Class 3-4 limits. In comparison, prEC 3 provides more continuous predictions for all load cases, but still reported significant unconservative results. Therefore, an original design approach based on the Overall Interaction Concept (O.I.C.) has been proposed. The latter suggests continuous local buckling curves for hot-rolled and welded I-sections in fire, covering a range from plastic to elastic to slender capacities. The O.I.C. proposals were shown to provide higher levels of accuracy, with all considered results never exceeding 6% on the unconservative side, which represents a significant improvement compared to the many and highly unsafe predictions provided by EC 3 and prEC 3. Besides, thanks to abandoning the classification concept and considering cross-sections as a whole, more accurate and consistent predictions have been reported for the O.I.C. proposal – for either compression or bending load cases, mean values as well as C.o.V.s of the $\chi_{L,O.I.C.} / \chi_{L,F.E.}$ ratios are significantly improved compared to the other two standards. Finally, the O.I.C.-based approach fulfills all three “reliability” criteria proposed by Kruppa, proving that the O.I.C.-based proposal can provide trustworthy predictions for the ultimate resistance of hot-rolled and welded I-sections at elevated temperatures.

Acknowledgements

Financial support awarded by the China Scholarship Council (C.S.C.) and the Natural Sciences and Engineering Research Council of Canada (N.S.E.R.C.) is gratefully acknowledged.

References

- Abaqus, G. (2011). "Abaqus 6.11." Dassault Systemes Simulia Corporation, Providence, RI, USA.
- Afshan, S., and Gardner, L. (2013). "The Continuous Strength Method for Structural Stainless Steel Design." *Thin-Walled Structures*, 68, pp. 42–49.
- AISC (2010). ANSI/AISC 360-10 - Specification for Structural Steel Buildings, American Institute of Steel Construction, Chicago, Ill.
- American Institute of Steel Construction (2017). Steel Construction Manual, 15th Edition.
- Ayrton, W. E., and Perry, J. (1886). "On Struts." *The Engineer*, 62.
- Ban, H., and Shi, G. (2018). "Overall Buckling Behaviour and Design of High-Strength Steel Welded Section Columns." *Journal of Constructional Steel Research*, 143, pp. 180–195.
- Ban, H., Shi, G., Shi, Y., and Wang, Y. (2013). "Residual Stress of 460MPa High Strength Steel Welded Box Section: Experimental Investigation and Modeling." *Thin-Walled Structures*, 64, pp. 73–82.
- Beg, D., and Kozlevčar, P. (2007). "Residual Stresses in Welded Elements Made of High Strength Steel." *ECCS TC8*, Doc. No. TC8-2007-006, Ghent.
- Boissonnade, N., Hayeck, M., Saloumi, E., and Nseir, J. (2017). "An Overall Interaction Concept for an Alternative Approach to Steel Members Design." *Journal of Constructional Steel Research*, 135, pp. 199–212.
- Bradford, M. A., and Liu, X. (2016). "Flexural-Torsional Buckling of High-Strength Steel Beams." *Journal of Constructional Steel Research*, 124, pp. 122–131.
- British Constructional Steelwork Association Ltd and Steel Construction Institute (2013). Handbook of Structural Steelwork: Eurocode Edition.
- Chen, J., and Young, B. (2008). "Design of High Strength Steel Columns at Elevated Temperatures." *Journal of Constructional Steel Research*, 64(6), pp. 689–703.
- Chen, J., Young, B., and Uy, B. (2006). "Behavior of High Strength Structural Steel at Elevated Temperatures."
- Chen, S., Fang, H., Liu, J., and Chan, T.-M. (2022). "Design for Local Buckling Behaviour of Welded High Strength Steel I-Sections under Bending." *Thin-Walled Structures*, 172, p. 108792.
- Choi, I.-R., Chung, K.-S., and Kim, D.-H. (2014). "Thermal and Mechanical Properties of High-Strength Structural Steel HSA800 at Elevated Temperatures." *Materials & Design*, 63, pp. 544–551.
- Couto, C., Coderre, T., Real, P. V., and Boissonnade, N. (2021). "Cross-Section Capacity of RHS and SHS at Elevated Temperatures: Comparison of Design Methodologies." *Structures*, Elsevier, pp. 198–214.
- Couto, C., and Real, P. V. (2019). "A Proposal Based on the Effective Section Factor for the Lateral-Torsional Buckling of Beams with Slender I-Shaped Welded Sections." *Thin-walled Structures*, 145, p. 106389.
- Couto, C., and Real, P. V. (2019). "Assessment of Eurocode Fire Design Rules for Structural Members Made of High Strength Steels." *Stability and Ductility of Steel Structures 2019: Proceedings of the International Colloquia on Stability and Ductility of Steel Structures (SDSS 2019)*, September 11-13, 2019, Prague, Czech Republic, CRC Press, p. 277.
- Couto, C., and Real, P. V. (2021). "The Influence of Imperfections in the Critical Temperature of I-Section Steel Members." *Journal of Constructional Steel Research*, 179, p. 106540.
- Couto, C., Real, P. V., Lopes, N., and Zhao, B. (2014). "Effective Width Method to Account for the Local Buckling of Steel Thin Plates at Elevated Temperatures." *Thin-Walled Structures*, 84, pp. 134–149.
- Couto, C., Real, P. V., Lopes, N., and Zhao, B. (2015). "Resistance of Steel Cross-Sections with Local Buckling at Elevated Temperatures." *Journal of Constructional Steel Research*, 109, pp. 101–114.

- Couto, C., Real, P. V., Lopes, N., and Zhao, B. (2016). “Numerical Investigation of the Lateral–Torsional Buckling of Beams with Slender Cross Sections for the Case of Fire.” *Engineering Structures*, 106, pp. 410–421.
- Coutu, C., Sanzel, A., Real, P. V., Lopes, N., and Zhao, B. (2016). “Beam-Columns with Thin Wall Cross-Sections in Case of Fire.” *Structures in Fire*.
- Eng, M. B. P. D., Uang, C.-M., and SE, R. S. (2011). *Ductile Design of Steel Structures*, McGraw-Hill Education.
- European Committee for Standardization (CEN) (2005). EN 1993-1-1: Eurocode 3 - Design of Steel Structures - Part 1-1: General Rules and Rules for Buildings.
- European Committee for Standardisation (CEN) (2006). EN 1993-1-5: Eurocode 3 - Design of Steel Structures - Part 1-5: Plated Structural Elements.
- European Committee for Standardisation (CEN) (2007). EN 1993-1-2: Eurocode 3 - Design of Steel Structures - Part 1-2: General Rules-Structural Fire Design.
- European Committee for Standardisation (CEN) (2020). PrEN 1993-1-2: Eurocode 3 - Design of Steel Structures - Part 1-2: General Rules-Structural Fire Design.
- Fang, H., and Chan, T.-M. (2018). “Axial Compressive Strength of Welded S460 Steel Columns at Elevated Temperatures.” *Thin-Walled Structures*, 129, pp. 213–224.
- Franssen, J.-M., Zhao, B., and Gernay, T. (2014). “Experimental Tests and Numerical Modelling on Eight Slender Steel Columns under Increasing Temperatures.” *8th International Conference “Structures in Fire”*, Tongji University Press, Shanghai, China.
- Franssen, J.-M., Zhao, B., and Gernay, T. (2016). “Experimental Tests and Numerical Modelling on Slender Steel Columns at High Temperatures.” *Journal of Structural Fire Engineering*, 7(1), pp. 30–40.
- Galambos, T. V., and Ketter, R. L. (1959). “Columns under Combined Bending and Thrust.” *Journal of the Engineering Mechanics Division*, 85(2), pp. 1–30.
- Gérard, L. (2020). “Contribution to the Design of Steel I and H-Sections Members by Means of the Overall Interaction Concept.” PhD thesis, Laval University.
- Gérard, L., Li, L., Kettler, M., and Boissonnade, N. (2019). “Recommendations on the Geometrical Imperfections Definition for the Resistance of I-Sections.” *Journal of Constructional Steel Research*, 162, p. 105716.
- Gérard, L., Li, L., Kettler, M., and Boissonnade, N. (2021). “Steel I-Sections Resistance under Compression or Bending by the Overall Interaction Concept.” *Journal of Constructional Steel Research*, 182, p. 106644.
- Hayeck, M. (2016). “Development of a New Design Method for Steel Hollow Section Members Resistance.” PhD thesis, University of Applied Sciences of Western Switzerland - Fribourg, University of Liège, Saint-Joseph University Beirut.
- Hayeck, M., Nseir, J., Saloumi, E., and Boissonnade, N. (2018). “Experimental Characterization of Steel Tubular Beam-Columns Resistance by Means of the Overall Interaction Concept.” *Thin-Walled Structures*, 128, pp. 92–107.
- Hirashima, T., and Uesugi, H. (2005). “Load-Bearing Capacity of H-Shaped Steel Columns under Local Buckling at Elevated Temperature.” *Fire Safety Science–Proceedings of the 8th International Symposium*, pp. 211–222.
- Hricak, J., Jandera, M., and Wald, F. (2014). “Local Buckling of Class 4 Cross-Sections at Elevated Temperatures.” Wald F. CE, Burgess I, Kwasniewski L, Horová K, editors. *Benchmark studies–experimental validation of numerical models in fire engineering*. Prague: CTU Publishing House, Czech Technical University, pp. 34–47.
- Johansson, B., Maquoi, R., Sedlacek, G., Müller, C., and Beg, D. (2007). “Commentary and Worked Examples to EN 1993-1-5 Plated Structural Elements.” JRC scientific and technical reports.
- Kodur, V. K. R., and Dwaikat, M. M. S. (2010). “Effect of High Temperature Creep on the Fire Response of Restrained Steel Beams.” *Materials and structures*, 43(10), pp. 1327–1341.
- Knobloch, M. (2008). “Local Buckling Behavior of Steel Sections Subjected to Fire.” *Fire Safety Science*, 9, pp. 1239–1254.

- Knobloch, M., Pauli, J., Somaini, D., and Fontana, M. (2013). “Stress–Strain Response and Cross-Sectional Capacity of Steel Sections in Fire.” *Proceedings of the Institution of Civil Engineers-Structures and Buildings*, 166(8), pp. 444–455.
- Kruppa, J. (1999). “Eurocodes–Fire Parts, Proposal for a Methodology to Check the Accuracy of Assessment Methods.” *CEN TC*, 250.
- Kucukler, M. (2021). “Local Stability of Normal and High Strength Steel Plates at Elevated Temperatures.” *Engineering Structures*, 243, p. 112528.
- Launert, B., Rhode, M., Pasternak, H., and Kannengießer, T. (2016). “Welding Residual Stresses in High Strength Steel: Experimental Results.” *Proceedings of the International Colloquium on Stability and Ductility of Steel Structures*, pp. 517–524.
- Li, L., and Boissonnade, N. (2022a). “Local/Global Coupled Instabilities of Slender I-Sections under Compression.” *Thin-Walled Structures*, 172, p. 108842.
- Li, L., Gérard, L., Kettler, M., and Boissonnade, N. (2022b). “The Overall Interaction Concept for the Design of Hot-Rolled and Welded I-Sections under Combined Loading.” *Thin-Walled Structures*, 172, p. 108623.
- Li, L., Gérard, L., Langlois, S., and Boissonnade, N. (2022c). “O.I.C.-Based Design of Mono-Symmetric I-Sections under Simple Load Cases.” *Thin-Walled Structures*, 174, p. 109134.
- Maia, É., Couto, C., Real, P. V., and Lopes, N. (2016). “Critical Temperatures of Class 4 Cross-Sections.” *Journal of Constructional Steel Research*, 121, pp. 370–382.
- Maquoi, R., and Rondal, J. (1978). “Mise En Équation Des Nouvelles Courbes Européennes de Flambement.” *Construction métallique*, 15(1), pp. 17–30.
- Maraveas, C. (2019). “Local Buckling of Steel Members under Fire Conditions: A Review.” *Fire Technology*, 55(1), pp. 51–80.
- Nseir, J. (2015). “Development of a New Design Method for the Cross-Section Capacity of Steel Hollow Sections.” PhD thesis, University of Applied Sciences of Western Switzerland - Fribourg, University of Liège, Saint-Joseph University Beirut.
- Pauli, J. (2013). “The Behaviour of Steel Columns in Fire: Material - Cross-Sectional Capacity - Column Buckling.” PhD thesis, Swiss Federal Institute of Technology Zurich.
- Petersen, C. (2012). *Stahlbau: Grundlagen der Berechnung und baulichen Ausbildung von Stahlbauten*, Springer-Verlag.
- Petersen, C. (2020). *Statik Und Stabilität Der Baukonstruktionen: Elasto-Und Plasto-Statistische Berechnungsverfahren Druckbeanspruchter Tragwerke: Nachweisformen Gegen Knicken, Kippen, Beulen*, Springer-Verlag.
- Prachar, M., Hricak, J., Jandera, M., Wald, F., and Zhao, B. (2016). “Experiments of Class 4 Open Section Beams at Elevated Temperature.” *Thin-Walled Structures*, 98, pp. 2–18.
- Real, P. V., Cazeli, R., da Silva, L. S., Santiago, A., and Piloto, e P. (2004). “The Effect of Residual Stresses in the Lateral-Torsional Buckling of Steel I-Beams at Elevated Temperature.” *Journal of Constructional Steel Research*, 60(3–5), pp. 783–793.
- Saloumi, E., Hayeck, M., Nseir, J., and Boissonnade, N. (2020). “Slenderness-Based Design Criteria to Allow for the Plastic Analysis of Tubular Beams.” *Journal of Constructional Steel Research*, 167, p. 105788.
- Schafer, B. W. (2008). “Review: The Direct Strength Method of Cold-Formed Steel Member Design.” *Journal of Constructional Steel Research*, 64(7–8), pp. 766–778.
- Shi, G., Zhang, Z., Zhou, L., Yang, L., and Zhou, W. (2020). “Experimental and Numerical Investigation on Local–Overall Interactive Buckling Behavior of Welded I-Section Steel Columns.” *Thin-Walled Structures*, 151, p. 106763.
- Su, A., Sun, Y., Zhao, O., and Liang, Y. (2021). “Local Buckling of S960 Ultra-High Strength Steel Welded I-Sections Subjected to Combined Compression and Major-Axis Bending.” *Engineering Structures*, 248, p. 113213.

- Sun, Y., Liang, Y., Zhao, O., and Young, B. (2021). "Experimental and Numerical Investigations of S690 High-Strength Steel Welded I-Sections under Combined Compression and Bending." *Journal of Structural Engineering*, 147(5), p. 04021054.
- Sun, Y., Su, A., Liang, Y., and Zhao, O. (2020). "Material Properties and Membrane Residual Stresses of S690 High Strength Steel Welded I-Sections after Exposure to Elevated Temperatures." *Thin-Walled Structures*, 152, p. 106723.
- Taras, A., and Greiner, R. (2008). "Torsional and Flexural Torsional Buckling—A Study on Laterally Restrained I-Sections." *Journal of constructional steel research*, 64(7–8), pp. 725–731.
- Theofanous, M., Profsert, T., Knobloch, M., and Gardner, L. (2016). "The Continuous Strength Method for Steel Cross-Section Design at Elevated Temperatures." *Thin-Walled Structures*, 98, pp. 94–102.
- Timoshenko, S. P., and Gere, J. M. (1963). *Theory of Elastic Stability*, Mc Graw Hill International Book Company.
- Wang, W., Kodur, V., Yang, X., and Li, G. (2014). "Experimental Study on Local Buckling of Axially Compressed Steel Stub Columns at Elevated Temperatures." *Thin-Walled Structures*, 82, pp. 33–45.
- Wang, W., Li, G., and Ge, Y. (2015). "Residual Stress Study on Welded Section of High Strength Q460 Steel after Fire Exposure." *Adv. Steel Construct*, 11, pp. 150–164.
- Wang, W., and Qin, S. (2016). "Experimental Investigation of Residual Stresses in Thin-Walled Welded H-Sections after Fire Exposure." *Thin-Walled Structures*, 101, pp. 109–119.
- Xiong, M.-X., and Liew, J. R. (2016). "Mechanical Properties of Heat-Treated High Tensile Structural Steel at Elevated Temperatures." *Thin-Walled Structures*, 98, pp. 169–176.
- Yan, X.-L., Li, G.-Q., Wang, Y.-B., and Jiang, J. (2020). "Experimental and Numerical Investigation on Flexural-Torsional Buckling of Q460 Steel Beams." *Journal of Constructional Steel Research*, 174, p. 106276.
- Yang, K.-C., Lee, H.-H., and Chan, O. (2006). "Performance of Steel H Columns Loaded under Uniform Temperature." *Journal of Constructional Steel Research*, 62(3), pp. 262–270.
- Yin, Y. Z., and Wang, Y. C. (2004). "A Numerical Study of Large Deflection Behaviour of Restrained Steel Beams at Elevated Temperatures." *Journal of Constructional Steel Research*, 60(7), pp. 1029–1047.
- Yun, X., Gardner, L., and Boissonnade, N. (2018a). "The Continuous Strength Method for the Design of Hot-Rolled Steel Cross-Sections." *Engineering Structures*, 157, pp. 179–191.
- Yun, X., Gardner, L., and Boissonnade, N. (2018b). "Ultimate Capacity of I-Sections under Combined Loading—Part 1: Experiments and FE Model Validation." *Journal of Constructional Steel Research*, 147, pp. 408–421.
- Yun, X., Gardner, L., and Boissonnade, N. (2018c). "Ultimate Capacity of I-Sections under Combined Loading—Part 2: Parametric Studies and CSM Design." *Journal of Constructional Steel Research*, 148, pp. 265–274.
- Yun, X., Saari, N., and Gardner, L. (2020). "Behaviour and Design of Eccentrically Loaded Hot-Rolled Steel SHS and RHS Stub Columns at Elevated Temperatures." *Thin-Walled Structures*, 149, p. 106646.
- Zieman, R. D. (2010). *Guide to Stability Design Criteria for Metal Structures*, John Wiley & Sons.